



**Michigan
Technological
University**

Michigan Technological University
Digital Commons @ Michigan Tech

Dissertations, Master's Theses and Master's Reports

2022

A Novel Pulsed-Plasma Catalytic Reactor for Dry Reforming of Methane


Benjamin F. Caithamer
Michigan Technological University, bfcaitha@mtu.edu

Copyright 2022 Benjamin F. Caithamer

Recommended Citation

Caithamer, Benjamin F., "A Novel Pulsed-Plasma Catalytic Reactor for Dry Reforming of Methane", Open Access Master's Thesis, Michigan Technological University, 2022.
<https://doi.org/10.37099/mtu.dc.etdr/1462>

Follow this and additional works at: <https://digitalcommons.mtu.edu/etdr>

 Part of the [Catalysis and Reaction Engineering Commons](#)

A NOVEL PULSED-PLASMA CATALYTIC REACTOR FOR DRY REFORMING OF
METHANE

By

Benjamin F. Caithamer

A THESIS

Submitted in partial fulfillment of the requirements for the degree of

MASTER OF SCIENCE

In Chemical Engineering

MICHIGAN TECHNOLOGICAL UNIVERSITY

2022

©2022 Benjamin F. Caithamer

This thesis has been approved in partial fulfillment of the requirements for the Degree of
MASTER OF SCIENCE in Chemical Engineering.

Department of Chemical Engineering

Thesis Advisor: *Michael Mullins*

Committee Member: *Pradeep Agrawal*

Committee Member: *Tony Rogers*

Department Chair: *Pradeep Agrawal*

Table of Contents

List of Figures	v
List of Tables	vii
Acknowledgements	viii
Abstract	ix
1 Background	1
1.1 Steam Methane Reforming	1
1.2 Thermal Dry Reforming	1
1.3 Plasma DRM	3
1.4 Catalysts for Plasma DRM	5
1.5 Motivation for Current Research	6
2 Experimental Setup	7
2.1 Catalyst Synthesis	7
2.2 HV-DC Pulse Forming Circuit	8
2.3 Power Calculations	11
2.4 Reactor Design and in situ Measurements	12
2.5 Experimental Procedure	15
3 Results	18
3.1 Catalyst Characterization	18
3.2 Catalyst Morphology and Composition	18
3.3 Emission Spectra	20
3.4 Quadrupole Mass Spectroscopy (QMS) Plots	22
3.5 Calculations	23
3.6 Methane Activation	24
3.6.1 Effect of Input Power	26
3.6.2 Catalyst Deactivation	31
3.6.3 Effect of Water	33
3.6.4 Effect of pulse width	34

3.6.5	Effect of Dilution Gas	36
3.7	Dry Reforming of Methane	39
3.7.1	Effect of catalyst and plasma alone	39
3.7.2	Effect of Catalyst Composition in DRM	42
3.7.3	Effect of Methane/CO ₂ ratio	46
4	Discussion	51
4.1	Methane Activation	51
4.2	Role of the Catalyst in DRM	54
4.3	Evidence for Reaction Mechanism based on Reactant Ratios	56
5	Conclusions	58
6	Recommendations	60
7	Reference List	62
A	Emission Spectra Reference Charts	69
B	Experimental Data	70
C	Extend of Reaction through Gibb's Free Energy Minimalization	83

List of Figures

Figure 1: Schematic of HV Pulse Forming Network.....	9
Figure 2: Example Oscilloscope Voltage and Current Pulse.....	10
Figure 3: Flow Schematic	12
Figure 4: Initial Reactor Drawing	14
Figure 5: Reactor Model	14
Figure 6: Reactor Details	15
Figure 7: Surface Morphology of the Copper Doped Catalyst.	19
Figure 8: Methane in Nitrogen.....	20
Figure 9: Methane in Argon.....	21
Figure 10: Methane and Carbon Dioxide in Argon	21
Figure 11: Example QMS Display.....	22
Figure 12: Conversion & Yield for all Catalysts at 65-75 Watts.....	25
Figure 13: Conversion & Yield for Copper Catalysts at 45-55 Watts.....	26
Figure 14: Conversion vs Power.....	28
Figure 15: Selectivity vs Power	29
Figure 16: Yield vs Power	30
Figure 17: ZnO Repeat Runs (Chronological Order)	31
Figure 18: First and Last ZnO Runs	32
Figure 19: Conversion vs Power for Different Pulse Widths (0.5, 1, and 2 μ s).....	35
Figure 20: Selectivity & Yield vs Power for Different Pulse Widths (0.5, 1, and 2 μ s) ...	36
Figure 21: Nitrogen at 55 Watts vs Argon at 25 Watts.....	39
Figure 22: Three Power Levels without Catalyst	40

Figure 23: Alumina without Discharge.....	41
Figure 24: CuO DRM	42
Figure 25: MnO DRM	43
Figure 26: ZnO DRM.....	45
Figure 27: NiO DRM.....	46
Figure 28: Low CO ₂ /Me ZnO DRM	47
Figure 29: Equal CO ₂ /Me ZnO DRM	48
Figure 30: High CO ₂ /Me ZnO DRM.....	49
Figure 31: Corona Discharge	53
Figure 32: Filamentous Brush Discharge	53
Figure 33: Spark Discharge over Catalyst	54

List of Tables

Table 1: Physical Characterization of Catalysts	18
Table 2: Chemical Characterization of Catalysts.....	19
Table 3: Methane Conversion vs Input Power.....	27
Table 5: Methane Conversion with Water	33
Table 6: Gas Plasma Properties	38
Table 7: Methane Bond Strengths.....	51

Acknowledgements

I'd like to thank and acknowledge all who have worked with me on this project. I thank my graduation committee for taking the time to review this work. I am extremely grateful to Michael Mullins for going above and beyond in assisting with both data collection and in the thesis writing process. I'd like to thank our machinist, Jerry Norkol, without whom none of these experiments would have been possible. I thank John Szczap for performing the various tests needed for catalyst characterization. Finally, I thank my family for their continual and unconditional support throughout.

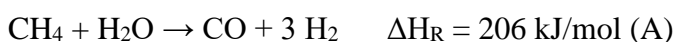
Abstract

Concerns over greenhouse gases have led to an increased interest in the Dry Reforming of Methane (DRM) which produces hydrogen and carbon monoxide from the reaction of two greenhouse gases (CO_2 and CH_4) over a catalyst. Currently, DRM is primarily a catalytic process which operates at temperatures between 700°C - 900°C , and 10 to 20 bar using a 1–1.5 ratio of CH_4/CO_2 . Unfortunately, these conditions also promote the water-gas shift reaction, which produces additional CO_2 . Catalyst coking and sintering can also be significant problems at these harsh conditions. We have developed a non-thermal, pulsed-plasma catalytic DRM reactor which operates at ambient temperatures and pressures. When combined with an integral monolithic catalyst bed this reactor demonstrated high conversions (60 to 80%) of both methane and carbon dioxide with high yields of hydrogen and carbon monoxide (30 to 80%). To achieve this, a novel solid-state, MOSFET-based HV pulse generator was developed with controllable rise times (4-20 ns), pulse duration (0.1 to 10 ms), pulse shape, and frequency (100 -10,000 Hz). This solid-state circuit provides improved operational flexibility and higher energy efficiency. The reactor incorporates a point-to-plane electrode arrangement with an integral monolithic catalyst cell which effectively places the catalyst in direct contact with the excited state plasma. The catalysts employed are copper oxides doped with a secondary metal oxide and are tailored for low-temperature plasma DRM reactions. Bench scale reactor tests were conducted using a feed of methane and/or carbon dioxide diluted in either nitrogen or argon. To evaluate the reaction kinetics, the partial pressure of the reactants and products were measured in real time via an on-line mass spectrometer, while the excited state species were simultaneously monitored using emission spectrometry. Tests were made with the plasma alone, and the plasma plus 4 different catalyst formulations. No significant reactions were observed for the plasma without a catalyst, or for the catalyst without a plasma. The reaction kinetics were measured for a range of input power, voltages, pulse length & frequency, and electrode geometries. The feed ratio of CO_2 to CH_4 was found to be of great significance in the overall conversion and the yield of hydrogen and CO, with near stoichiometric reactant ratios proving to be the best. The stoichiometric ratio of carbon monoxide to hydrogen in the products depended on the combination of the metal oxides employed and to the strength of reactant adsorption on the catalyst surface. Based on the observed kinetics and emission spectroscopy results, we propose a surface moderated reaction model which explains the high reactant conversions and product yields observed. Estimates of the energy efficiency of the bench-scale process, and rate of reaction indicate the potential of this novel reactor for practical applications.

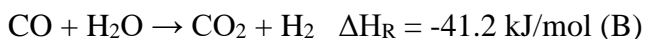
1 Background

1.1 Steam Methane Reforming

Steam methane reforming (SMR) to produce hydrogen from natural gas and other fossil fuels is currently the cheapest source of industrial hydrogen and accounts for approximately 95% of the US production of hydrogen [1]. This process proceeds in two stages. First, high-temperature (700-1000°C) steam reacts with methane over a catalyst at high-pressures (3-25 bar) to form syngas:



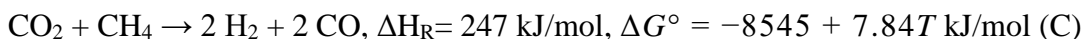
This is usually followed by further hydrogen generation in the water-gas shift reaction at milder conditions (250 to 350°C):



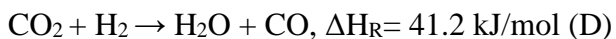
The major downside to SMR is the creation of CO₂ and other greenhouse gases, for each ton of hydrogen produced, 9 to 12 tons of CO₂ are created. Additionally, methane is often burned to supply energy for reaction A.

1.2 Thermal Dry Reforming

Concerns over greenhouse gases (e.g., methane and carbon dioxide) have increased interest in finding green chemistries that utilize greenhouse gases [2]. A potential green alternative to SMR is Dry Reforming of Methane (DRM), which produces hydrogen and carbon monoxide from the reaction of CO₂ with methane over a catalyst. DRM also holds promise for improved utilization of biogas and natural gas with high ratios of CO₂ to methane. Wang [3] reports the associated enthalpies and free energies for the DRM reactions of importance. For DRM the primary reaction is:

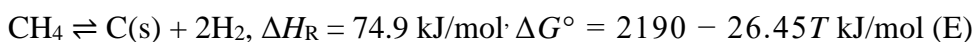


Here, two greenhouse gases are the reactants and useful syngas, with a theoretical 1:1 molar ratio of H₂ and CO is produced. This reaction path produces less CO₂ than SMR, but may yield less hydrogen, since the hydrogen produced can further react with carbon dioxide producing water and more carbon monoxide.



Currently, DRM is a catalytic process operated at temperatures between 700°C - 900°C, and 10 to 20 bar using a 1–1.5 ratio of CH₄/CO₂. Pakhare, et al. [4] report that under these conditions up to a 50% yield of hydrogen (>25% conversion of methane) may be obtained. Unfortunately, these are also temperatures and pressures which promote the water-gas shift reaction, which produces additional CO₂.

Conversion of methane to other useful products is complicated by the relative stability of the saturated methane molecule. Activation of the C-H bond via thermal or catalytic means to produce higher hydrocarbons or alcohols has usually resulted in poor yields and selectivity, primarily due to the relatively severe reaction conditions required to activate the C-H bonds. The process can lead to the formation of carbon on the catalyst surface in several ways.



In addition to the carbon formation, sintering is prevalent which further reduces the activity of the catalyst. Lavoie [5] and le Sache [6] have done excellent reviews of thermal/catalytic DRM processes, with special attention to the thermodynamics of conversion and the unfavorable conversions and yields associated with the temperatures and pressure requirements.

1.3 Plasma DRM

An alternative method to promote DRM is via a non-thermal plasma (NTP) catalytic reaction operating at moderate temperatures and pressures. Bogaerts and Centi [7] have published an in-depth review on the principles of plasma activated reactions for CO₂. Typically, the plasma is generated by an electrical discharge in the gas phase reactants, which activates the gas molecules forming ions, radicals and excited state molecules which permit reactions to occur at milder temperatures and pressures than traditional methods. Standard thermal equilibrium models of chemistry and reaction mechanisms are less relevant due to the non-equilibrium concentration of the excited species. This approach is of particular interest for DRM since only the reactant electrons are activated without the need to heat the entire gas phase (Snoeckx and Bogaerts [8]). Plasma excitation of methane via a plasma discharge has disadvantages as well, since the recombination of the excited state radicals produced in the plasma is a chaotic and an uncontrolled process. Much greater product selectivity can be achieved via combining a plasma with a catalyst. This can be accomplished either by a two-step process, placing the catalyst downstream of the plasma, or by placing the catalyst in situ with the plasma. Of the two, in situ is preferable as the exciting state species are short-lived, and the catalyst can have various synergistic effects which stabilize both the plasma and the excited state species, as well as help control the recombination to desired products. This non-equilibrium reaction process opens an entirely new range of exciting chemistries.

A variety of plasma assisted DRM approaches have been investigated, including corona discharges, microwave (MW) plasmas, dielectric barrier discharges (DBDs), gliding arc (GA) plasmas, atmospheric pressure glow discharges (APGDs), and nanosecond-pulsed discharges (NPD). Seyed-Matin et al. [9] have investigated the carbon dioxide reforming of methane to synthesis gas in a DC-pulsed plasma without a catalyst at ambient temperatures and pressures. At an input energy of about 11 eV they measured a feed conversion of 38% for CH₄ and 28% for CO₂ with a selectivity of 74% for H₂ and CO. Bak et al. [10] found that small amounts of methane form from a CO₂/CO/H₂ mixture in a nanosecond pulsed DBD reactor; this means in DRM the methane will reach an

equilibrium concentration instead of reacting to completion. Numerous plasma catalysis studies have been conducted with DBD plasma reactors in a packed-bed configuration, where the packing is coated with catalyst materials. Sekine et al. [11] have shown that DBD systems have lower electron energies than pulse discharge plasma and have a much lower energy efficiency than NPD systems. Cheng, et al. [12] reported studies on combination pulsed DBD packed bed reactors that show better conversions than with continuous DBD reactors. Zhao et al. [13] reported that the rate of methane conversion in pulsed corona reactors is higher than DBD based reactors and inferred that appropriately designed pulsed corona discharge reactors are a potentially improved alternative for methane reactions such as DRM. Mei et al. [14] used a four-factor five-level central composited design ANOVA analysis to find optimal plasma parameters for DBD DRM over a Ni/Al₂O₃ catalyst. Feed gas flow rate, feed gas CH₄/CO₂ ratio, power, and Ni loading % were selected as the independent variables. They noticed a tradeoff between product yields and energy efficiency, and ultimately concluded that the optimal conditions were at a power input of 60 watts, 56 ml/min flow rate, feed gas ratio of 1, and nickel loading of 9.5%. They recently followed up with another study [15], this time without a catalyst and employing an artificial neural network (ANN) to compute a model of the system. The same variables were studied, except catalyst loading was replaced with discharge length. Here they found that the feed gas ratio was by far the most important parameter for conversion, selectivity, and energy efficiency. Using the ANN, they were able to accurately predict the majority of the results. Being able to produce models such as this will be important if these processes are ever to be industrialized.

Kuznetsov et al. [16] investigated the methane conversion in mixtures of CH₄–CO₂ and CH₄–O₂ via pulsed nanosecond discharges without a catalyst. Methane conversion to CO and H₂ was measured for spark, diffuse, and corona discharge, with the most efficient DRM occurring in spark discharges with the shortest pulse duration. They estimated an energy cost of conversion of one CH₄ molecule with CO₂ of approximately 15 electron volts per molecule. Sun et al. [17] similarly investigated the differences in plasma discharge types for a negative pulsed plasma for methane cracking and found practically no conversion is obtained for corona, 10% is obtained for streamer discharge and 45-75%

conversion for spark discharge with streamer and spark having similar energy efficiencies. Abieve et al. [18] discuss a range of plasma and photo-assisted catalytic DRM techniques and review the substantial research to date.

The ability to effectively couple the discharge energy in the plasma in the presence of a catalytic substrate is key to making such pathways feasible; however, new catalysts designed specifically for this application are required. Andersen et al. [19] and Brune et al. [20] report several potential catalysts for plasma DRM in DBD reactors and concluded that the presence of a catalyst in the discharge zone led to lower conversions than plasma alone, except for Pt/Al₂O₃, where the conversion was similar to the plasma-only. Tu et al. [21] examined a Ni/Al₂O₃ catalyst with three different packing configurations in a DBD reactor and showed a significant effect of particle shape and packing density. Zhang et al. [22] studied both an empty DBD reactor and a packed DBD where a Cu–Ni/Al₂O₃ catalyst filled the discharge gap. They observed that a significant synergism between the catalyst and DBD plasma was achieved. Conversions of CH₄ for plasma alone, plasma-catalysis and catalysis alone were 13%, 69% and 10%, respectively. The associated selectivity to CO and H₂ for the combined plasma-catalytic process were 76% and 57%. In other studies, the development and application of novel catalysts for NTP-DRM has led to improvements in conversions, product distribution and yields [23-27]. However, few of these studies offer experimental or theoretical evidence for the mechanism by which these catalysts work.

1.4 Catalysts for Plasma DRM

A variety of catalysts are described in the extensive literature on thermal DRM reactions. (Puliyalil [28]) Copper-based catalysts are widely used for thermal CO₂ hydrogenation to CH₃OH synthesis (240–260°C and 40–50 bar) from CO₂. Cu-based catalysts have been modified with various metal oxides (e.g., Zn, Ni) for the hydrogenation of CO₂ (Eliasson [29], Gao et al. [30]) However, the thermodynamics of the reaction results in low selectivity at higher conversions.

In the case of plasma-assisted catalysis, high conversions of CO_2 and CH_4 are achieved even at mild operating conditions and due to the non-equilibrium characteristics of the NTP which promotes thermodynamically unfavorable chemical reactions (Song et al. [31]). Placing the catalyst directly in contact with the discharge zone creates a synergistic effect between NTP and the catalyst on the yield and selectivity (Chung and Chang [33]). Sheng et al. have published an excellent analysis of the interaction of the plasma with catalyst surfaces [34]. They indicate that the plasma assists in overcoming the dissociative adsorption barrier for methane. They deduce that this activation lowers the activation energy of the DRM process from 91 kJ/mol to 44.7 kJ/mole over the catalysts they studied. The activation of CO_2 in a plasma discharge has also been examined by Berthelot and Bogaerts [35] and several others have detailed the mechanism for molecular activation of DRM mixtures of CO_2 and CH_4 . [36-38].

1.5 Motivation for Current Research

This current study is unique compared to the previous work cited in the literature in that a series of DRM experiments has been conducted using a positive pulsed DC discharge in conjunction with a novel reactor configuration which places the catalyst directly in contact with the plasma. For this new application, DRM thermal catalysts and plasma DRM catalysts previously examined in the literature do not exhibit the activity or selectivity needed for a practical DRM plasma catalysis system. Consequently, for this study we have developed a new set of DRM catalysts specifically designed and tested for use at near ambient conditions while placed in contact with the active discharge region. Of equal significance, a new solid-state HV pulse forming network has been developed with fast rise times, variable pulse duration, and a wide range of pulse frequency control, and is described herein. The reactor is combined with methods that allow real-time, in-situ sampling and measurement of the reactive species and products. Using these new tools, a systematic study of the DRM plasma catalysis process over a set of copper-based mixed metal oxide catalysts has been conducted. A series of reactor tests were conducted for both methane cracking and DRM at different initial reactant concentrations and residence times over a range of voltages, pulse lengths & frequencies.

2 Experimental Setup

Coupling an integral mixed oxide catalyst bed with the active zone of a pulsed-plasma discharge permits gas-phase synthesis processes and non-equilibrium conversions not accessible via thermal or traditional catalytic routes. In this study, the dry reforming of methane (DRM) under a DC pulsed plasma discharge coupled directly with new plasma DRM catalysts was examined in a batch reactor. Novel alumina-supported, copper-based catalysts designed specifically for this application were developed, characterized, and tested. To permit more careful control of the discharge energy delivered to the reactor, a new solid-state HV-DC pulse forming network was developed which generates carefully tailored pulses and measurement of the applied discharge voltage and current, pulse frequency and duration, and rise times on the nanosecond scale. The composition of the gas-phase was continuously monitored in situ in real-time via a Quadrupole Mass Spectrometer (QMS) to measure the reactant conversions and product yields. A fiber optic cable placed close to the discharge zone was connected to an emission spectrometer, and the plasma emission spectra were also recorded in situ during operation. Using this arrangement, the influence of the reactor process conditions (including the discharge characteristics, catalyst composition, CH_4/CO_2 ratio, etc.) on conversions and yields were measured.

2.1 Catalyst Synthesis

Several catalyst formulations with a generic composition of $\text{Cu}_x\text{M}_y\text{O}_z/\text{Al}_2\text{O}_3$ have been synthesized for this study. In addition to a plain copper oxide doped alumina, several secondary metals were used in binary combinations with copper including Ni, Mn, and Zn. In all the tests an activated alumina support (BASF CPN activated alumina 8-14 mesh) was impregnated with the desired mixed metal oxide composition using the traditional incipient wetness technique. The targeted stoichiometric ratio of metals was 1:1 (x:y). Using the nitrate salts of the corresponding metals, an aqueous solution with the desired stoichiometric ratio of metals was prepared and applied to the alumina substrate using a pipette until the solid support was saturated. The saturated support was dried at

150°C overnight, and then calcined in a muffle furnace at 600°C for 2 hours in the presence of air. The samples were weighed before and after impregnation to estimate the total catalyst loading. The process was then repeated until an approximately 10% weight increase for the catalyst plus support was attained.

Extensive characterization of the catalysts was conducted post-synthesis to verify the metal loading and stoichiometry, catalyst structure, surface area, and other physical properties. The alumina substrate and alumina/catalyst surface areas and pore structures were determined using a Micromeritics® ASAP2020. The morphology and crystalline state of the final catalysts were examined via both SEM imaging and X-ray Diffraction (XRD). The elemental composition and metals ratio of the catalysts as prepared were determined via EDAX surface mapping and x-ray fluorescence spectroscopy (XRF). A non-porous alumina ceramic tube was used as an interchangeable annular catalyst holder which could be fitted into the discharge zone of the reactor. The adsorption isotherms for carbon dioxide and methane on the alumina support and the metal-doped catalyst samples were measured at 25°C and a range of absolute pressures from 0.1 kPa to 101 kPa using a Cahn Vacuum microbalance to quantify the amount of adsorbed reactants.

2.2 HV-DC Pulse Forming Circuit

In a pulsed plasma reactor, high voltage pulse discharges (1 to 20 kV) with fast rise times (<5ns) and short durations (0.1 to 10 μ s) are needed to impart high electron energies to excited state species without sufficient time to induce thermal molecular modes in the gas phase. With the production of sufficiently energetic electrons (4 to 12 eV), excited states for both methane and carbon dioxide may be produced at ambient gas-phase temperatures and pressures. Mechanical switches or spark gaps combined with capacitors do not allow sufficient control over the pulse shape, rise times, duration, and frequency, and thus the energy delivered is equally difficult to control. Also, for analog HV pulse forming networks, the overall reactor circuit design affects the discharge characteristics in unpredictable ways. To obtain finer control over the discharge energy and characteristics, a solid state digitally controlled pulse forming network is desirable. We

could not find any commercially available HV-DC pulsed solid-state systems with the capabilities we were looking for; therefore, we designed and custom-built a nanosecond solid-state HV-DC pulse generator as shown in Figure 1 (Lim [39]).

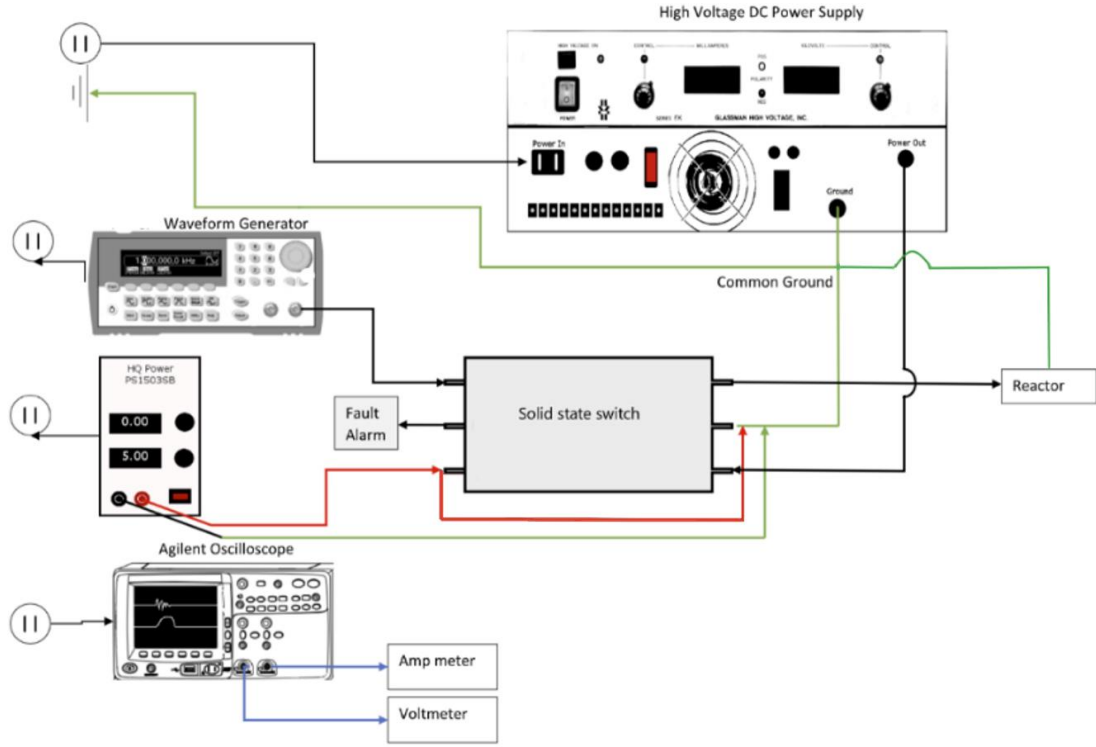


Figure 1: Schematic of HV Pulse Forming Network

The principal HV power supply is a Glassman series EK HV power supply (0-30kV) which is coupled to a solid-state Behlke fast HV Push-pull MOSFET switch HTS 201-03-GSM with response times < 5 ns. The switch is powered by a HQ Power PS1503SB DC power supply (± 10 V), and the pulse frequency, rise times, and duration controlled by an Agilent 33220A 20MHz Arbitrary Waveform Generator. The applied voltage and current to the reactor were measured using a Tektronix P6015A HV probe and a Pearson Electronic wide band current transformer connected to an Agilent DSO6012A 100MHz Digital storage oscilloscope. This solid-state HV-DC pulse generator can accurately control pulse rise times, duration, shape, and pulse frequency.

It offers considerable improvement over mechanical rotating spark gap or thyatron pulse generating designs in terms of energy input, flexibility, simplicity of operation, and process control. This new solid-state system can tune the discharge energy input and electron energy in a way the older designs cannot. A sample oscilloscope output signal for the voltage and current measurement delivered to the reactor is shown in Figure 2.

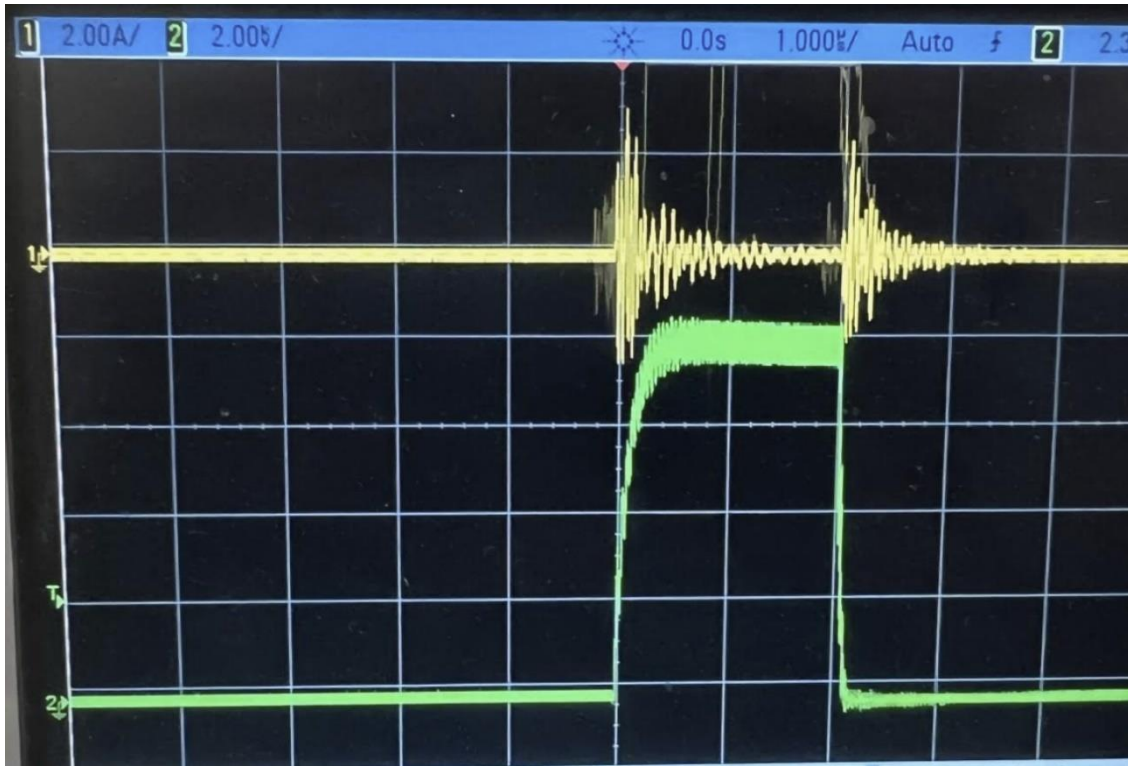


Figure 2: Example Oscilloscope Voltage and Current Pulse

2.3 Power Calculations

The average power applied to the reactor can be estimated from the voltage (kV) and current (mA) displayed on the console of the Glassman HV power supply. However, the actual power applied is a function of the peak pulse voltage, the peak current, the pulse frequency, and the pulse duration. The digital storage oscilloscope was used to measure all of these, plus the average current over time. To determine the power delivered to the reactor more accurately, the current and voltage was measured at the reactor using a HV probe attached to the needle electrode and a current ring was connected to the ground side electrode wire. Using this technique, we were able to deliver almost square HV pulses with fast rise times (<5 to 20 ns), that compared well with the applied voltage on the power supply. By comparison, the instantaneous peak current measurement was much higher (e.g., 0.1 to 3 A), than the average current delivered by the power supply (3 to 10 mA). The current pulses are less well defined than the voltage, with considerable “ringing” depending on the design of the circuit and reactor electrode configuration. This “ringing” is due to the EMP generated by the reactor, which easily travels through the metal cladding of the sensor’s cable. The voltage jitters during streamer/spark discharge is due to the individual filaments. Both this “jitter” and the ring effects can be observed in the oscilloscope readings in Figure 2. Therefore, although the average power applied to the reactor was between 2 and 80 watts, the instantaneous power could exceed 15 kW. For a comparison of the applied to delivered power, we estimate a power delivery efficiency of 75% to 85% .

2.4 Reactor Design and in situ Measurements

A schematic of the reactor and associated flow equipment is shown in Figure 3. The reactor is contained within a testing chamber to provide environmental control and

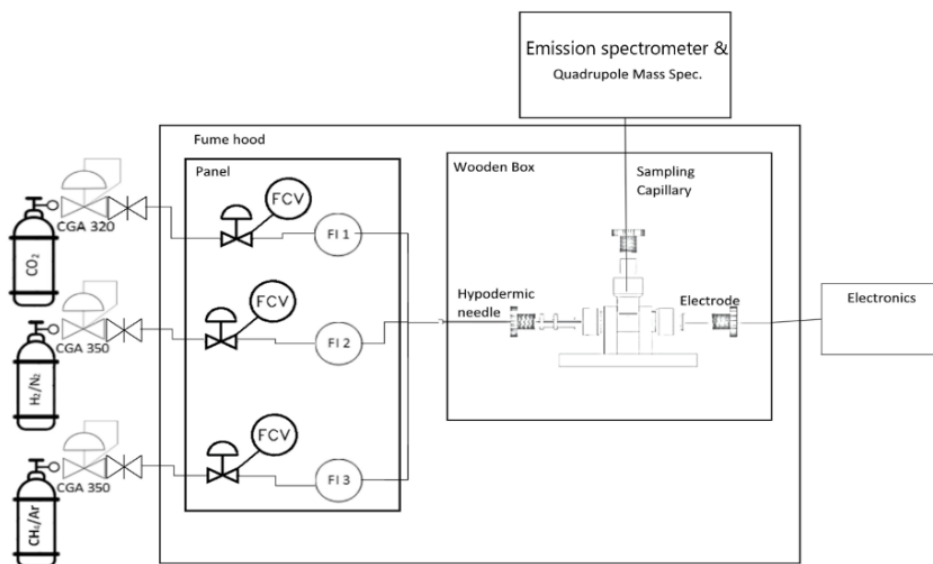


Figure 3: Flow Schematic

provide additional safety while working with the HV equipment. This novel pulsed plasma catalytic reactor operates at atmospheric or slightly higher pressure, and at moderate to low temperatures (<50°C). It can be operated in either batch or flow mode, though batch mode was studied more intensively. The test gases were high purity CO₂, 3% CH₄ in argon, 3% CH₄ in nitrogen, 3% hydrogen in nitrogen (for calibration purposes), and CO calibration gases in nitrogen at several concentrations (Matheson specialty gases). Concentrations of CH₄ and H₂ were always kept below the LFL levels (4% H₂ & 4% CH₄) for safety reasons. The gas flows are controlled by a set of Swagelok Nupro[®] needle valves and measured via a set of Cole Palmer[®] brand rotameters.

The initial reactor was constructed out of a T-shaped Ace Glass Adapter 5829012; it has three threaded 1-inch diameter openings. A point to plane electrode configuration was employed with a #10 hypodermic needle as the active electrode (positive) and a 2 cm porous disc as the ground electrode. The hypodermic needle electrode also acts as the gas

inlet, and the outlet gas passes through the porous frit to the gas exit. There are needle valves on the entrance and exit to allow operation in either continuous or batch modes. The electrode needle can be adjusted to allow for an electrode spacing up to 2 cm, although a spacing of between 1 and 1.5 cm was typically employed. The crushed catalyst particles were attached to a non-porous alumina ceramic tube. An interchangeable annular ring (1 cm ID) was used to center the catalysts tubes in the active discharge region. Alternatively, catalyst pellets could be poured directly into the reaction area through the top port, in which case the reactor was only filled approximately halfway as to not interfere with gas flow or discharge visibility. The top port of the reactor was used as the instrument port. A Teflon cylinder was used to partially fill the dead space of the instrument port. The instrument port allows for insertion of a sampling capillary directly into the active plasma region in addition to a fiber optic probe.

A 5-meter sampling capillary is directed to the Dycor MA200MDEF quadrupole mass spectrometer (QMS) which continuously monitors the partial pressures of up to 5 desired reaction species in real-time. The QMS measures 6 points per second and records the average value every second. Alternatively, the QMS can be run in analog mode which can track all species AMU 1-100 simultaneously, however this mode severely reduces the sampling rate to approximately once every 30 seconds and thus was not used extensively. The length of the sampling capillary allows for ample space between the reactor and the QMS, which is important as the plasma discharge produces an Electro-Magnetic Pulse (EMP) effect that interferes with nearby digital electronics.

The port was also used to insert a fiber optic probe (Stellarnet F400 μ m 3-meters) to collect emission spectra from the plasma zone using a Black Comet Stellarnet UV-VIS-NIR Spectrometer. The end of the fiber optic cable was placed 1-cm directly above the active discharge region; therefore, the fiber optic cable had to be sufficiently long to prevent EMP interference. Additionally, the fiber optic cable had to be custom designed without its steel monocoil shielding as the effective range of the EMP was greatly extended through the steel cladding of the cable.

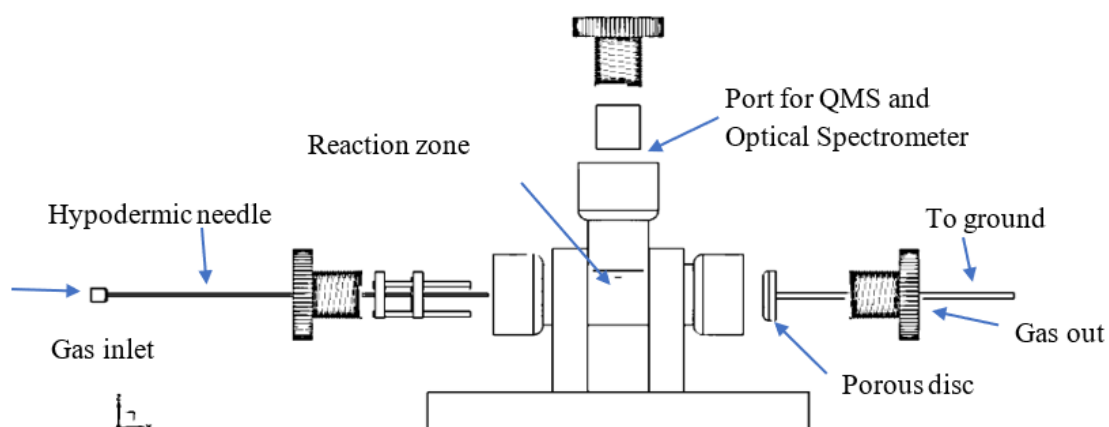


Figure 4: Initial Reactor Drawing

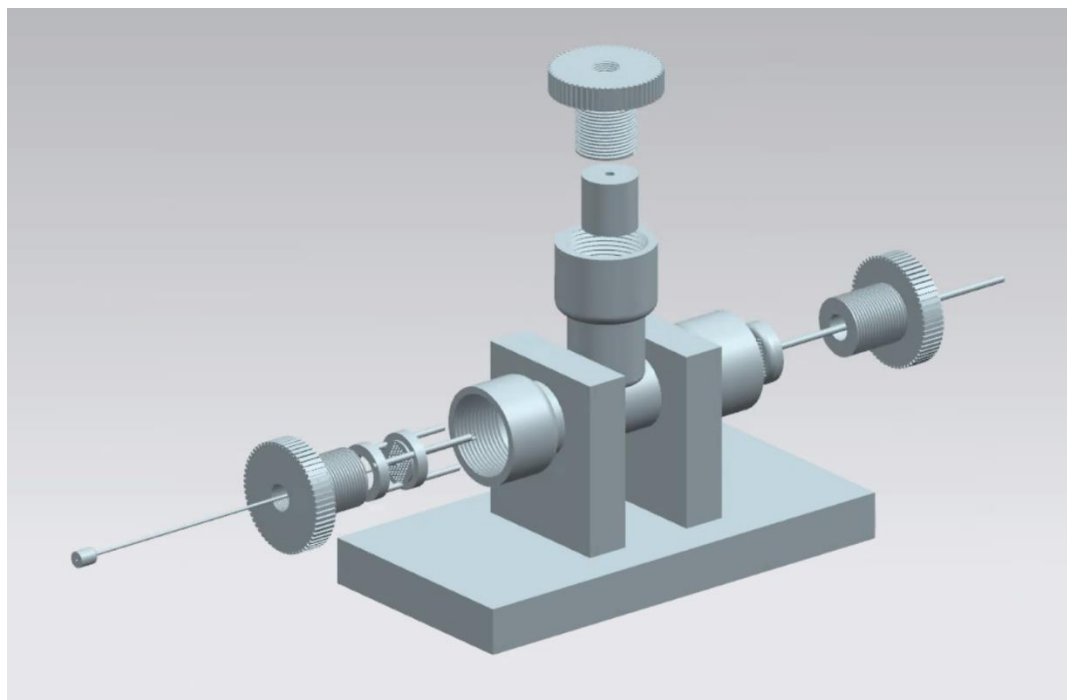


Figure 5: Reactor Model

After the initial methane activation tests, a new reactor was designed to reduce the reactor's dead space and improve response time by using a significantly smaller reactor

volume (25 ml to 5 ml). The new reactor body consists of a 3.8 cm OD/ 2.5 cm ID by 10 cm long Lexan tube with PTFE threaded inserts at either end fitted with inlet and outlet gas fittings and feedthrough ports for the active HV electrode and ground. The reactor dead space outside the electrodes was further minimized using machined PTFE blocks, creating a total reactor working volume of 5 cm³. The electrode, flow patterns, and catalyst configuration were unchanged. A schematic drawing of the initial reactor design is shown in Figure 4 and a 3D model in Figure 5; a detailed figure of the redesigned reactor is shown in Figure 6.

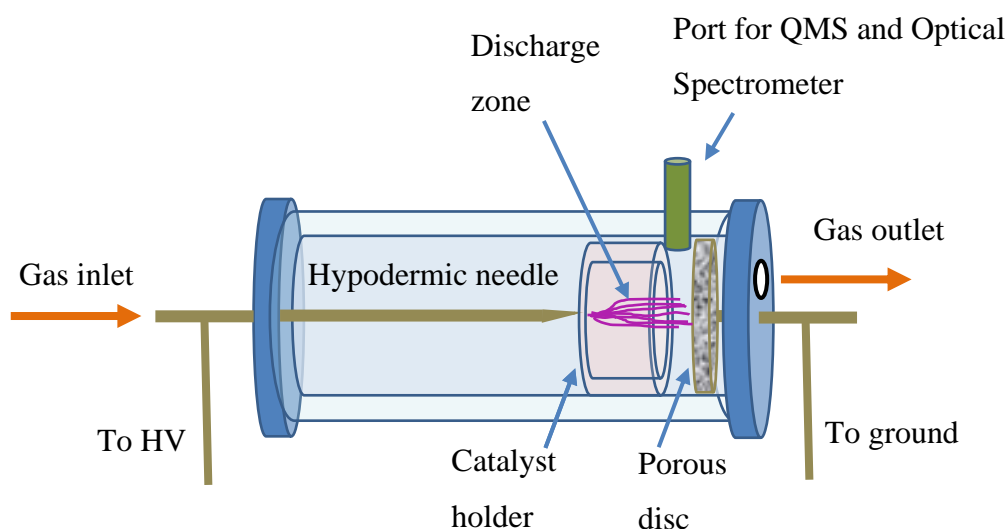


Figure 6: Reactor Details

2.5 Experimental Procedure

Most of the tests can be categorized as either methane cracking or DRM. In both cases the reactor was operated in batch mode; this was primarily done to increase measurement sensitivity. It also removes the necessity of predicting an appropriate flow rate for each run and reduces gas consumption. However, batch mode has the downside of introducing transient effects such as adsorption, which complicates analysis.

For methane cracking, the reactor was flushed with the feed methane/nitrogen feed gas at 200 ml/min for 5-10 minutes between runs to allow for the removal of products from the previous run, and for the gas to adsorb onto the catalyst particles. The reactor's inlet and outlet valves were then closed in quick succession; the outlet was always closed first to prevent any possible backflow. Data collection via the QMS was then started and readings were allowed to stabilize for 100-200 seconds prior to initiation of the electrical discharge. The plasma was then applied for 600 seconds, and data was collected for an additional 100-200 seconds after the plasma was shut off. The QMS can track 5 species simultaneously, for methane cracking runs methane and hydrogen were obviously tracked—the other three species were varied between runs to monitor for potential byproducts or likely contaminants. The presence of water was studied in several tests by running the feed gas through a water-filled gas washing flask. The delivered plasma power was controlled by varying the pulse frequency instead of voltage as recommended by Song et al. [31]. Frequency was typically set between 1400-2300 Hz while the other parameters were typically fixed at the following values: voltage at 10 kV, amperage at 5 mA, rise time <5ns, pulse duration at 1 μ S and the discharge gap at 12.5 mm.

The QMS's ability to track multiple species live allows for substantially more data to be collected than with alternative methods such as GCMS. However, it is not without its downsides; it is unable to differentiate between species with the same molar mass and can only detect unadsorbed gas phase species. In DRM tests, argon was used as a dilutant instead of nitrogen to account for nitrogen and carbon monoxide having the same molar mass.

A slightly different operating procedure was used for the DRM studies. The reactor was flushed with the feed CH_4/Ar gas for 5-10 minutes. Carbon dioxide was then added to the feed gas via a needle valve until the desired CO_2/CH_4 ratio was obtained as measured via the QMS. After flushing, the reactor was isolated in the same manner as in cracking. Several minutes had to be allowed for the CO_2 to equilibrate prior to plasma ignition, as in addition to adsorbing onto the alumina support, CO_2 can also chemisorb onto the copper oxide of the catalyst to form copper carbonate complexes [32]. Significant CO_2

adsorption was observed for all tested catalysts. Methane also adsorbs onto the catalyst, but in significantly smaller quantities.

The electrical discharge settings were pre-set to the desired power input based upon the voltage (3 to 10 kV), frequency (1 to 10 kHz), pulse rise time ($<5\text{ns}$), and pulse duration (.2 to $5\mu\text{s}$). After initiating the discharge, the reaction species were followed until completion of the reaction was observed via QMS, approximately 200 to 1200 sec. All the electrical input parameters were obtained from the oscilloscope and power supply readings, and the output from the QMS was recorded digitally to a laptop computer.

3 Results

3.1 Catalyst Characterization

A set of catalysts with the general composition of $\text{Cu}_x\text{M}_y\text{O}_z/\text{Al}_2\text{O}_3$ was synthesized for this study. The catalysts and support were physically analyzed using BET surface area analysis; CO_2 and methane adsorption studies; and particle density measurements. The results for these tests are summarized in Table 1.

Table 1: Physical Characterization of Catalysts

Catalyst/substrate	Al_2O_3 support	CuO doped	Cu/Zn doped	Cu/Mn doped	Cu/Ni doped
BET surface area (m^2/g)	315	212	208	206	245
Catalyst porosity	.66	0.61	0.62	0.62	0.65
Average pore radii (angstroms)	50	44	44	45	46
Catalyst density (g/cm^3)	2.5	2.6	2.6	2.6	2.5

3.2 Catalyst Morphology and Composition

The chemical structure and elemental composition were further characterized via XRD, SEM, and x-ray fluorescence (XRF). All the catalysts have been examined via SEM to determine the surface morphology. As shown in Figure 7, the surface of the Cu doped alumina has a large degree of microporosity in tandem with the extremely fine micropore structure.

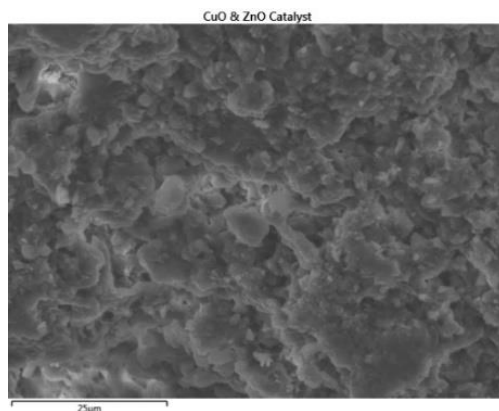


Figure 7: Surface Morphology of the Copper Doped Catalyst.

The catalysts were prepared by using stoichiometric ratios of each metal in a nitrate solution using the incipient wetness method. The dried and calcined catalysts were then tested for the actual final elemental composition as prepared using XRF and EDAX surface analysis. The XRF results were measured on finely crushed samples of the original catalyst are therefore more representative of the bulk composition of the catalyst. The results for the XRF tests for each catalyst type are shown in Table 2.

Table 2: Chemical Characterization of Catalysts

Catalyst Dopant	Cu (average)	Cu/Zn (average)	Cu/Mn (average)	Cu/Ni (average)
Al (mol %)	81.3	80.1	82.6	86.6
Cu (mol %)	17.4	9.5	9.6	5.1
Zn (mol %)	0.1	9.3	-	-
Mn (mol %)	-	-	6.6	-
Ni (mol %)	-	-	0.2	7.4
Trace (mol %)	1.2	0.1	1.0	0.9

3.3 Emission Spectra

The excited state species generated during the pulsed plasma discharge were measured in situ using emission spectroscopy. Emission spectra were first obtained for the methane in nitrogen and methane in argon. The emission spectra for methane in nitrogen is shown below in Figure 8. The peaks between 350 and 450 nm are associated with the excited states for methane radicals, with large peaks at 490 nm and 650 nm associated with atomic hydrogen. The peaks between 550 nm and 600 nm and at long wavelengths (>700 nm) are due to excited states of nitrogen.

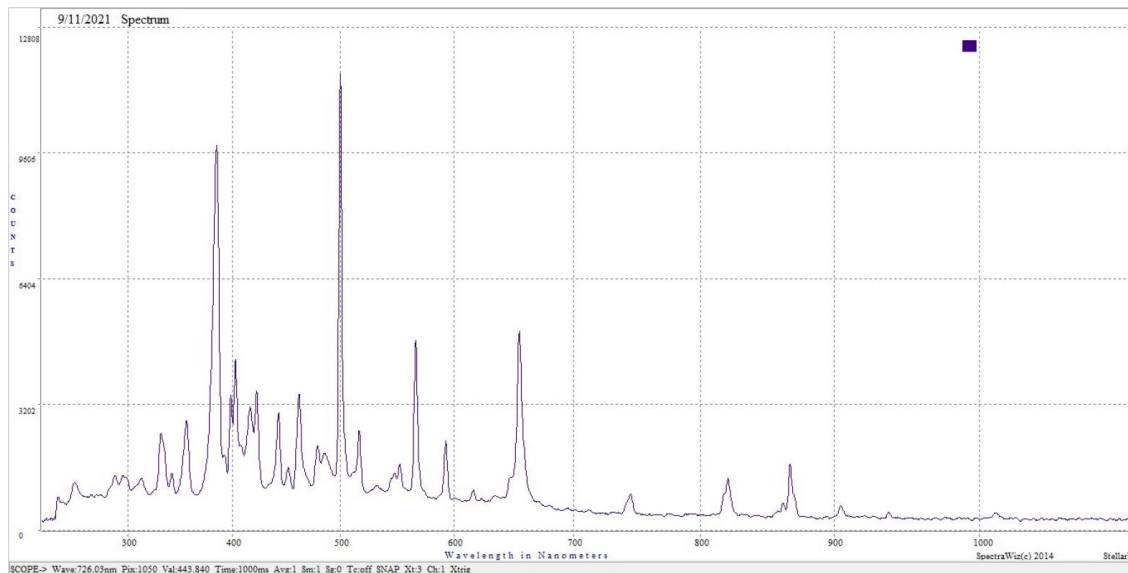


Figure 8: Methane in Nitrogen

The results for emission spectra from methane in argon are similarly shown below in Figure 9. The peaks for methane and atomic hydrogen are the same as the previous figure, however the peaks for nitrogen have been replaced by those corresponding to argon between 750 and 920 nm.

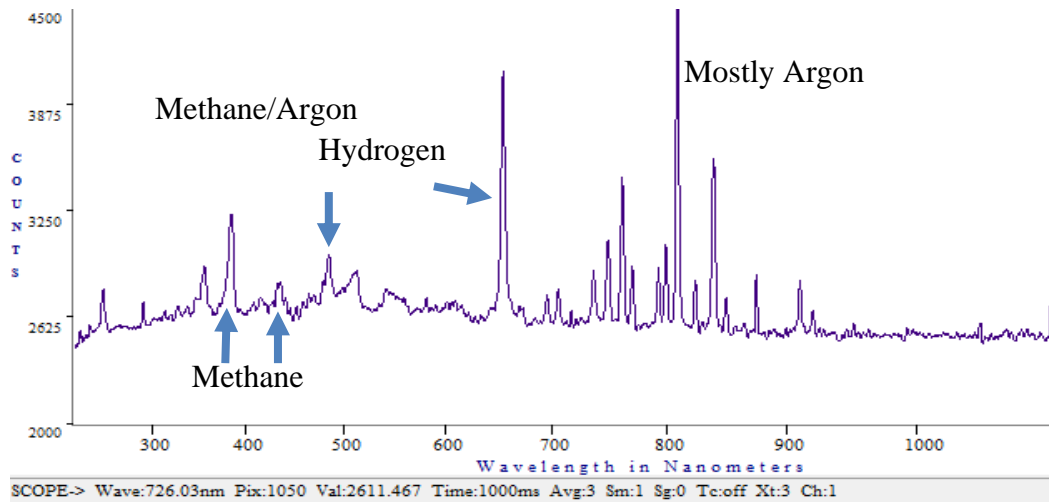


Figure 9: Methane in Argon

The emission spectra for methane, argon, and carbon dioxide are shown below in Figure 10. Several new emission peaks may be noticed, particularly between 430 and 490 nm, and around 780 nm. Carbon dioxide has a large ability to absorb the available electrons, and thus reduce the concentration of methane and argon excited state species.

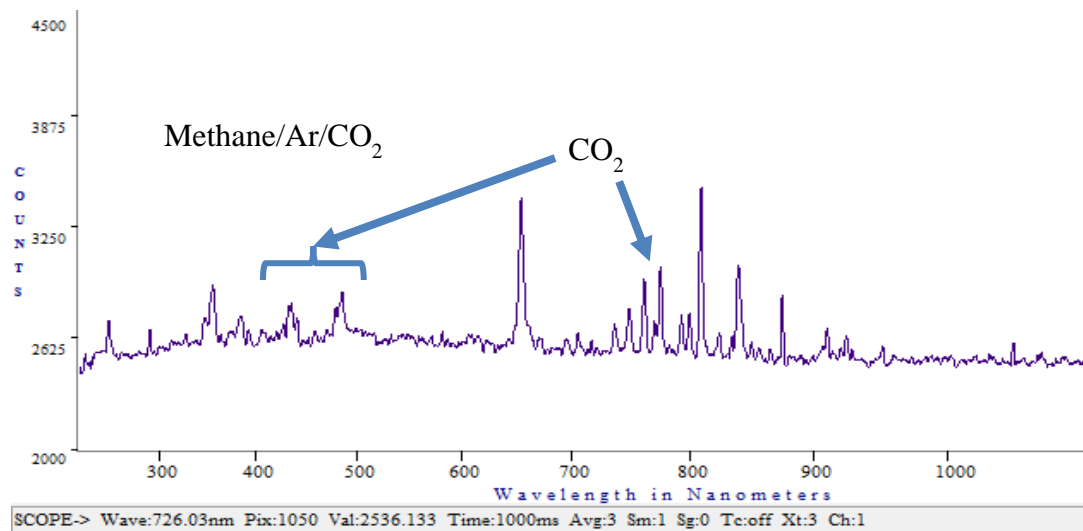


Figure 10: Methane and Carbon Dioxide in Argon

3.4 Quadrupole Mass Spectroscopy (QMS) Plots

The gas-phase composition in the reactor was measured in real time via an on-line quadrupole MS (Dycor/Ametek). A fine fused silica sampling capillary (50 μm ID/150 μm OD) was run directly from the plasma reactor zone to the quadrupole sampling chamber. Scans over a range of 1 to 100 amu were run for each test. The output can be viewed either in a discrete analog mode or as a function of pressure versus time for up to 5 species continuously. The QMS takes 6 pressure samples each second per species and records the average of these values as in a graph plotted against time. All of the data were acquired via a modified RS-232 data port and saved to an external computer hard drive using a MATLAB program. An example of the pressure-time graph is shown in Figure 11. There is some electronic noise due to the HV pulsed circuit, however, the data can be further averaged and smoothed during the signal processing, so each point shown on the resulting graphs is the average of 20-200 measurements. On the plots, the individual species partial pressures were normalized to the initially calibrated CH_4 pressures ($\sim 3\%$ concentration). Calibration runs were also conducted for hydrogen (3%) under similar circumstances.

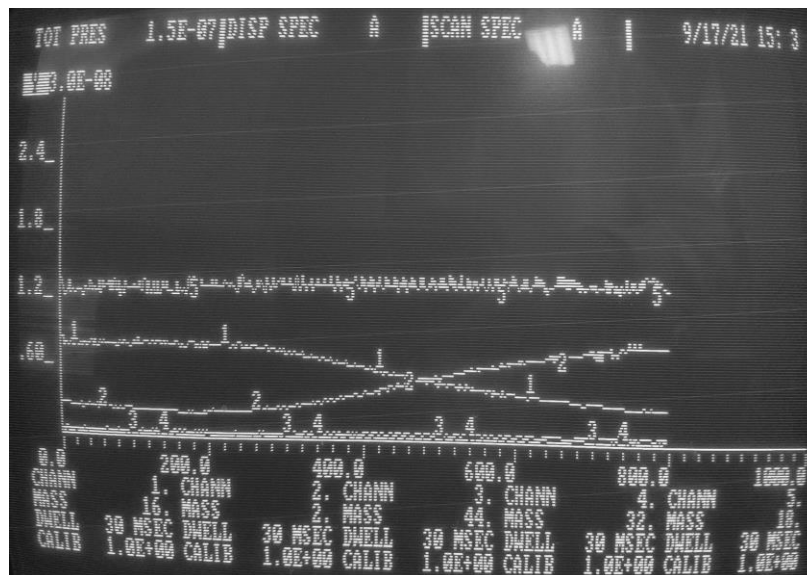


Figure 11: Example QMS Display

3.5 Calculations

The conversion of each reactant can be calculated from the QMS plots as shown below

$$X_{CH_4}(\%) = \frac{CH_4_{consumed}}{CH_4_{initial}} \cdot 100 \quad (1)$$

$$X_{CO_2}(\%) = \frac{CO_2_{consumed}}{CO_2_{initial}} \cdot 100 \quad (2)$$

The percent yield of hydrogen can be calculated via equation 3

$$Y_{H_2}(\%) = \frac{H_2_{produced}}{2 \cdot CH_4_{initial}} \cdot 100 \quad (3)$$

The percent yield of carbon monoxide can be calculated by either the carbon balance as shown in equation 4, or the oxygen balance as shown in equation 5. The carbon-based yields are reported in this study, although both methods yield similar results.

$$Y_{CO_{carbon}}(\%) = \frac{CO_{produced}}{CH_4_{initial} + CO_2_{initial}} \cdot 100 \quad (4)$$

$$Y_{CO_{oxygen}}(\%) = \frac{CO_{produced}}{2 \cdot CO_2_{initial}} \cdot 100 \quad (5)$$

The selectivity of the products can be calculated by equations 6 and 7.

$$S_{H_2}(\%) = \frac{H_2_{produced}}{2 \cdot X_{CH_4} \cdot CH_4_{initial}} \cdot 100 = \frac{Y_{H_2}}{X_{CH_4}} \quad (6)$$

$$S_{CO}(\%) = \frac{CO_{produced}}{CH_4_{consumed} + CO_2_{consumed}} \cdot 100 = \frac{Y_{CO} \cdot (CH_4_{initial} + CO_2_{initial})}{CH_4_{consumed} + CO_2_{consumed}} \quad (7)$$

Specific energy input (SEI) is commonly defined as the ratio of power input to gas flow rate and is reported in J/ml as shown in equation 8 or in electron volts per molecule as in equation 9. (Debek, et al. [27])

$$SEI \left(\frac{J}{ml} \right) = \frac{Power(W)}{Flow \left(\frac{ml}{s} \right)} \quad (8)$$

$$SEI \left(\frac{eV}{molecule} \right) = SEI \left(\frac{J}{ml} \right) \cdot \frac{6.241 \cdot 10^{21} \left(\frac{eV}{kJ} \right) \cdot 22.4 \left(\frac{L}{mol} \right)}{6.023 \cdot 10^{23} \left(\frac{molecule}{mol} \right)} \quad (9)$$

Most of our experiments were run in batch mode, so the flow term in equation 8 was replaced with the reaction volume divided by the plasma on time, as shown in equation 10.

$$SEI \left(\frac{J}{ml} \right) = \frac{P(W) \cdot t_{plasma}(s)}{V_{reactor}(ml)} \quad (10)$$

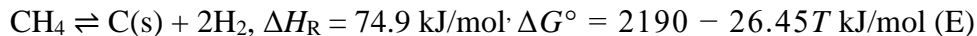
Energy efficiency can be defined in several different ways. In this study the energy conversion efficiency (ECE) will be defined as the ratio of the lower heating values (LHV) of the products to those of the reactants plus the input energy, as shown in equations 11 and 12. (Wang et al. [40]) Due to the magnitude of the LHVs, ECE for methane cracking reaches a theoretical maximum of 60%.

$$ECE_{cracking} (\%) = \frac{LHV_{H_2} \left(\frac{kJ}{mol} \right) \cdot H_2 produced \left(\frac{mol}{s} \right)}{LHV_{CH_4} \left(\frac{kJ}{mol} \right) \cdot CH_4 consumed \left(\frac{mol}{s} \right) + L + P \left(\frac{kJ}{s} \right)} \quad (11)$$

$$ECE_{DRM} (\%) = \frac{LHV_{H_2} \left(\frac{kJ}{mol} \right) \cdot H_2 produced \left(\frac{mol}{s} \right) + LHV_{CO} \left(\frac{kJ}{s} \right) \cdot CO produced \left(\frac{mol}{s} \right)}{LHV_{CH_4} \left(\frac{kJ}{mol} \right) \cdot CH_4 consumed \left(\frac{mol}{s} \right) + LHV_{CO_2} \left(\frac{kJ}{mol} \right) \cdot CO_2 consumed \left(\frac{mol}{s} \right) + P \left(\frac{kJ}{s} \right)} \quad (12)$$

3.6 Methane Activation

The ability to activate methane is critically important for any subsequent reactions. Thus, each catalysts' ability to activate methane was assessed by its performance in the methane cracking reaction (E). In addition to the four copper-oxide based catalysts prepared for this study, a plain alumina tube is included as a blank.



At low power levels the plasma discharge forms a corona, at these conditions negligible conversion was obtained for every catalyst. At higher power inputs the discharge transitions into streamers and then quickly into spark discharges. The transitions between the plasma types are gradual with overlap between the regimes. The conversion of methane and yield of hydrogen for each catalyst is shown below at approximately 65 watts, which is well within the streamer/spark discharge regime.

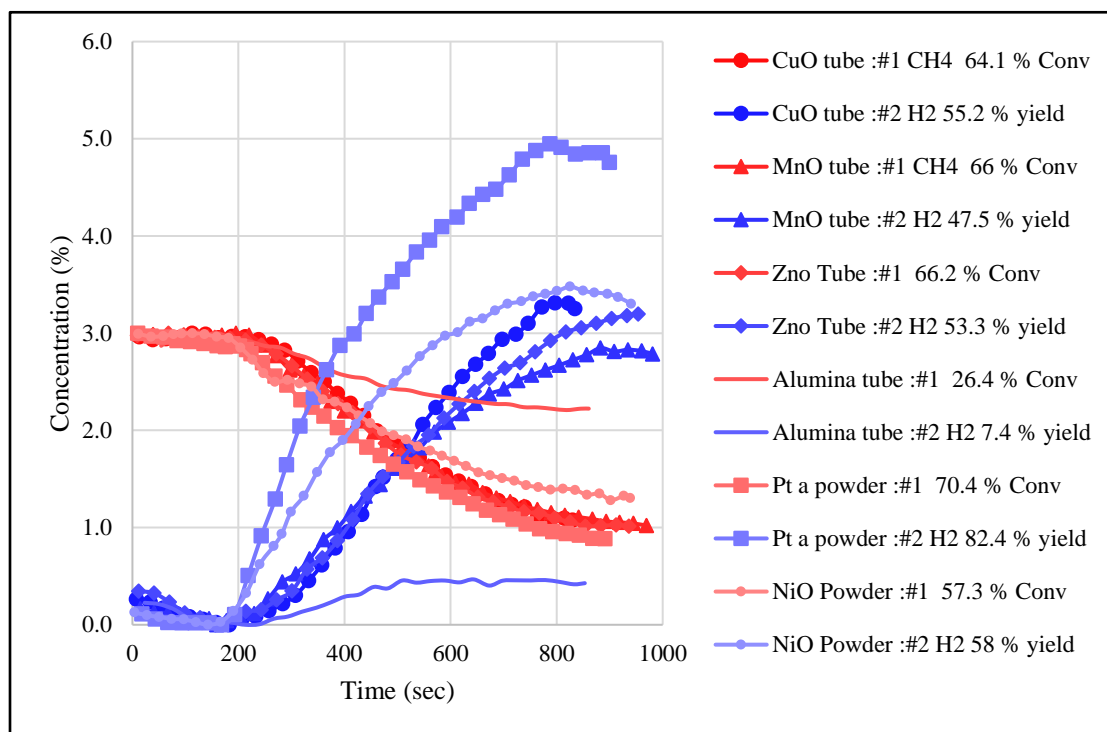


Figure 12: Conversion & Yield for all Catalysts at 65-75 Watts

As seen in Figure 12, all catalysts greatly outperform the plain alumina and substantial conversion (50-70%) is obtained for all catalysts. At this power level the performance of the CuO, CuO/ZnO, and CuO/MnO catalysts all have comparable conversions, while the CuO/NiO is slightly inferior. Platinum is a well-known catalyst for methane activation but is unsuitable for DRM as it is easily poisoned by CO and is thus not of great interest to this study. A single platinum run was included here to act as a performance benchmark for the CuO based catalysts. The platinum unsurprisingly outperformed any of the copper-based catalysts, but only by a small margin. There is a greater disparity in

hydrogen yields between the catalyst, but they follow a similar trend; the platinum catalyst has the best hydrogen yield while the NiO/CuO and MnO/CuO catalysts have the lowest yields.

3.6.1 Effect of Input Power

Both the conversion and yield results vary heavily with the input power level. To demonstrate this, the copper catalysts are shown again in Figure 13, this time at a lower power level.

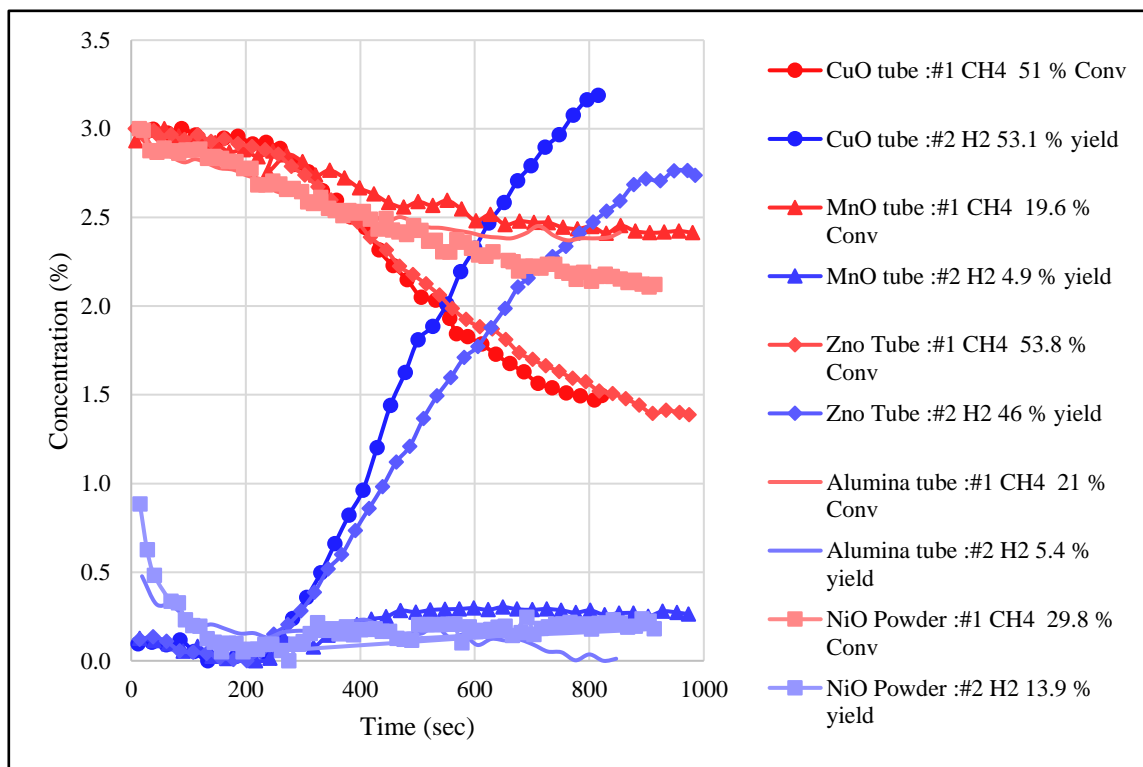


Figure 13: Conversion & Yield for Copper Catalysts at 45-55 Watts

Here the results are drastically different. The MnO catalyst shows no improvement in either methane conversion or hydrogen yield over the plain alumina; the NiO catalyst is similarly suppressed and only shows a slight improvement over the alumina. In contrast the CuO catalyst shows only a slight decrease in conversion from the higher power level and the ZnO catalyst is hardly affected at all. The reason for this is visually apparent upon observing the reaction—for both the MnO and NiO catalysts the streamer discharges are unstable and infrequent, while the streamers are still stable and continuous

for both the ZnO and CuO catalysts. This suggests that the ZnO and CuO catalysts have a synergistic affect with the plasma that reduces its breakdown voltage or increases the mean electron energy; allowing streamers to be generated at lower power levels leading to increased conversion at low input powers. This could be a substantial benefit as being able to run at lower energy levels would lead to increased energy efficiency.

The approximate methane conversion for each catalyst for different power levels is shown in below in Table 3. At 25 watts none of the catalysts produce streamers, but CuO/ZnO produces a visibly stronger corona discharge. At 45-55 watts MnO and NiO produce intermittent streamers while CuO and CuO/ZnO produce continuous streamers. Above 55 watts all catalysts produce strong streamers and sparks. The results are summarized in the following Table 3.

Table 3: Methane Conversion vs Input Power

Watts	Alumina	CuO	CuO/MnO	CuO/ZnO	CuO/NiO
25	3.2%	2.3%	0.62%	16%	X
45	20%	51%	23%	54%	X
55	20%	56%	55%	62%	27%
65	24%	64%	66%	66%	55%
75	24%	74%	70%	69%	85%

Overall, it seems that once stable streamers or sparks are obtained, conversion increases almost linearly with input power. The addition of ZnO to the CuO catalyst improves plasma stability and thus conversions at lower wattages but doesn't have a substantial impact on conversion at higher wattages. The addition of MnO has the opposite effect, reducing plasma stability and conversion at lower wattage levels, while yielding comparable conversions to CuO and CuO/ZnO at higher wattages. While NiO data were

not collected below 50 watts, it appears to have a similar effect as MnO with substantially increased activity at high power levels.

The methane conversion and hydrogen selectivity/yield are shown in Figure 14, Figure 15, and Figure 16.

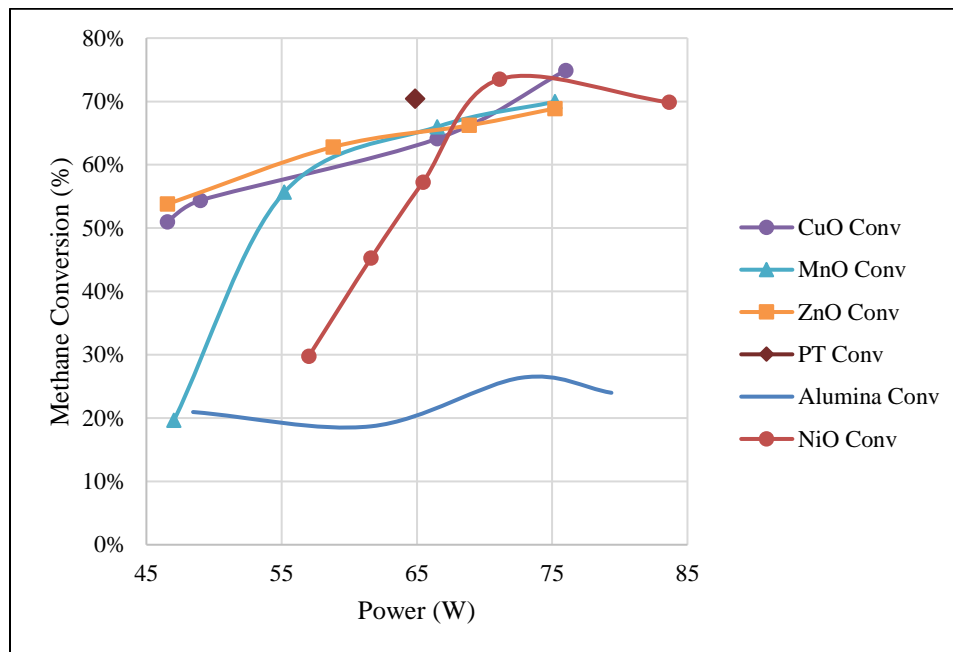


Figure 14: Conversion vs Power

The selectivity, yield and conversion for the MnO/CuO catalyst drastically increase over 45-55 watts; above this the selectivity remains constant, while the conversion and yield increased in a roughly linear fashion. The ZnO/CuO catalyst's selectivity is also mostly constant but shows a slight decrease at higher power levels. This decrease in selectivity is most likely caused by the formation of either higher hydrocarbons, methanol, or water. In this case, higher hydrocarbons are most likely, as the only source of oxygen would be through reduction of the catalyst metals. The CuO hydrogen selectivity and yields drop significantly at higher power levels, suggesting a greater amount of byproducts are being formed. Another explanation for hydrogen selectivity deviating from 100% is that methane is adsorbing onto the catalyst during the run leading to an over estimation of conversion and subsequent under estimations of selectivity and yield. The catalysts were

pre-adsorbed with methane before each run; however, this pre-adsorption could have been incomplete due to insufficient pre-flush times, or it's possible that the presence of plasma increases the catalysts adsorption capability leading to subsequent adsorption. This is a better explanation for the very low selectivities of the plain alumina and low wattage MnO runs, as the majority of the observed “conversion” could be adsorption resulting in little to no hydrogen production. Interestingly, this can also explain abnormally high selectivity observed for the NiO doped catalyst, as any pre-adsorbed methane is not detected on the QMS but could still react, contributing to hydrogen production and causing an apparent increase in selectivity and yield. This is the best explanation for selectivity values over 100%. It is likely that both byproduct formation and methane adsorption are occurring, as neither alone can account for the wide range of hydrogen selectivities observed.

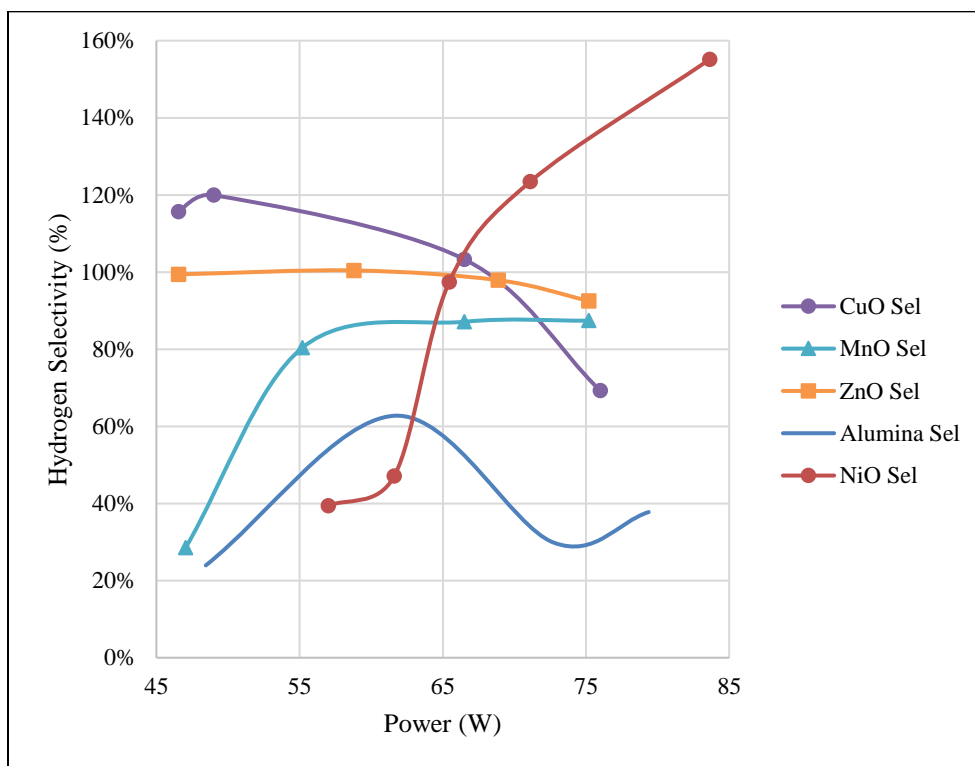


Figure 15: Selectivity vs Power

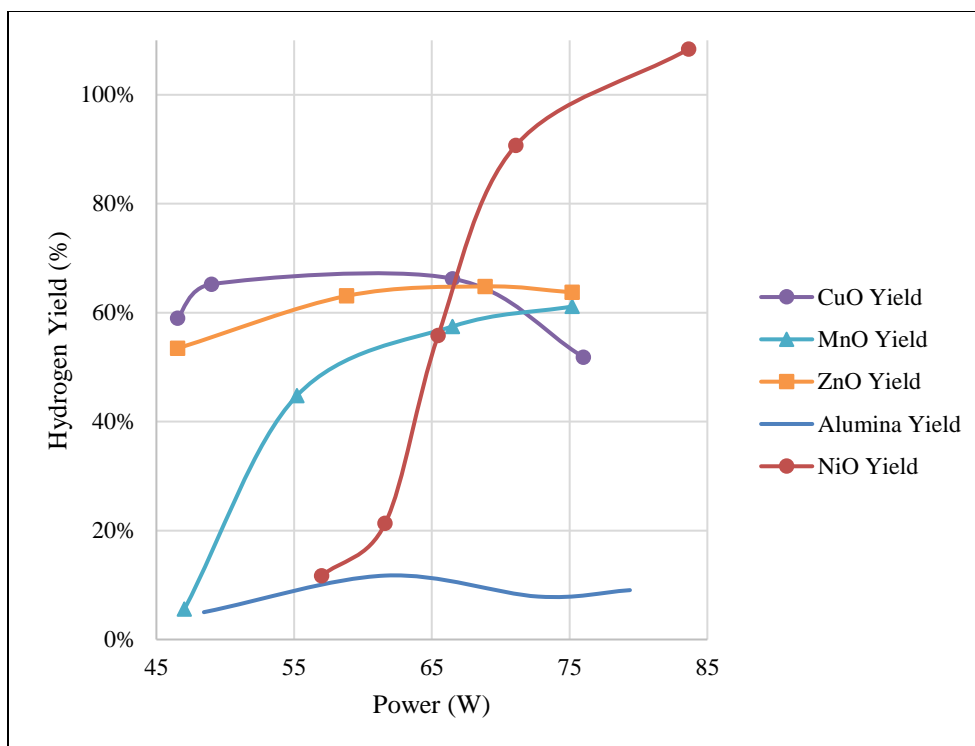


Figure 16: Yield vs Power

The NiO catalysts conversion increases significantly from 55-70 watts, after which it levels out around 70%, however the hydrogen yield continues to increase to 108% leading to very high selectivities over 150%. This suggests that more preadsorbed methane reacts with the NiO doped catalyst than with the other catalysts.

3.6.2 Catalyst Deactivation

The cracking reaction for methane activation also produces solid carbon, which can deposit on the catalyst, causing deactivation through coking. Ideally catalyst lifetime tests would be performed, but this is beyond the scope of this study. Additionally, as solids cannot be detected via the QMS, there were no available means of quantifying carbon deposition. However, solid carbon was confirmed via visible accumulation on the cathode and catalyst. Catalyst deactivation was expected to be seen in Figure 17, which shows four consecutive identical runs of the same catalyst with identical power inputs, however, the conversion unexpectedly increased slightly. This increase may in part be attributed to a slight increase in temperature due to insufficient cooling time allowed

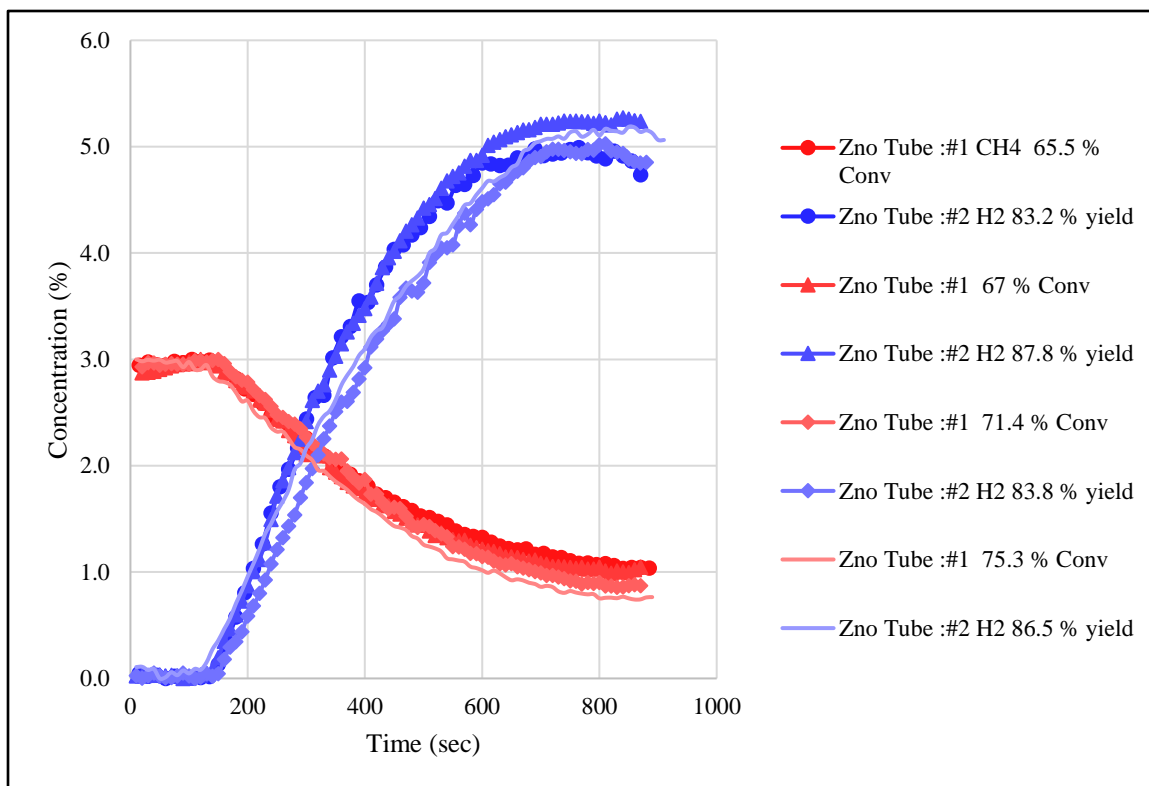


Figure 17: ZnO Repeat Runs (Chronological Order)

between runs. The general effect of temperature on the plasma DRM system needs further investigation for confirmation of the thermal effects.

The catalyst deactivation can be more readily observed in Figure 18 which shows the first and last of numerous runs of the ZnO catalyst. The first run had 20% higher conversion than the last run despite running at a mere fraction of the last runs power. However, no specific conclusions may be drawn due to other operating parameters that varied slightly between runs.

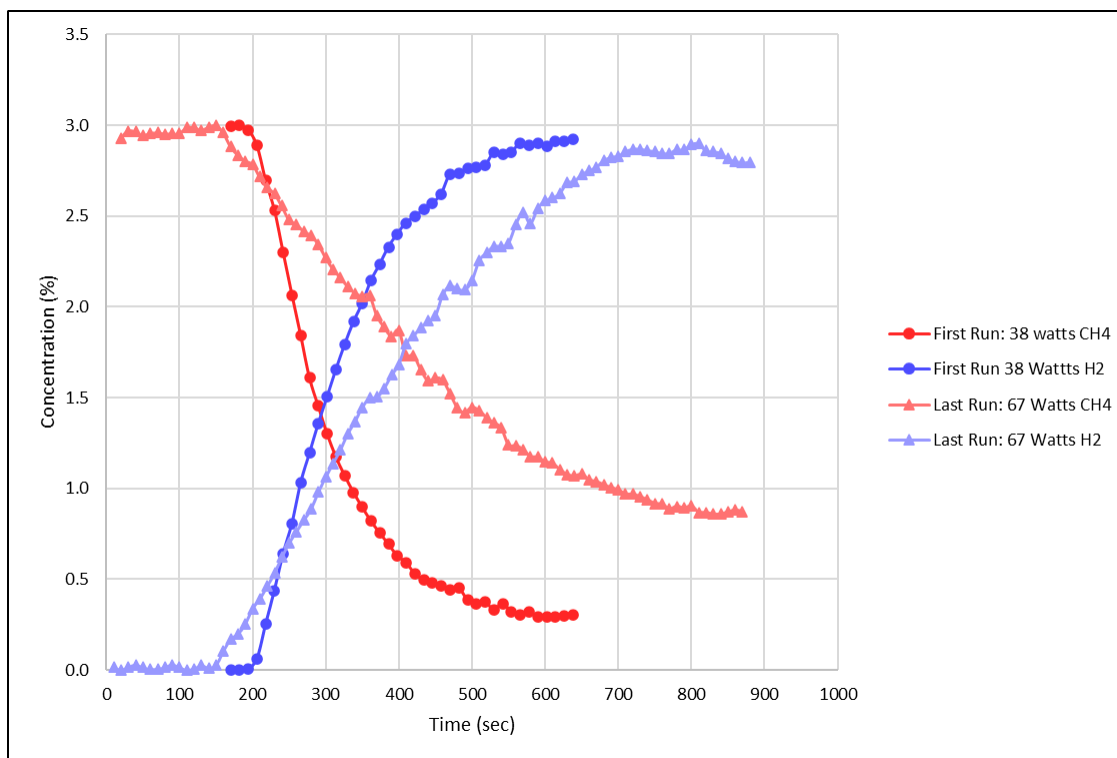


Figure 18: First and Last ZnO Runs

Considering that catalyst deactivation can only be observed when comparing the first few runs of a catalyst, it can be concluded that fresh catalysts initially deactivate very quickly, after which the deactivation slows to an undetectable level for the short time durations of this study. A plausible theory is that only the most active sites (caused by uneven distribution of the catalyst particles, or by proximity to the plasma source) of the catalyst directly reduce methane to carbon, while the rest only partially reduce it to methyl ions and radicals which then proceed to react in the gas phase. The most active sites would

then be quickly deactivated by coking, while the remaining active sites would last substantially longer.

3.6.3 Effect of Water

The addition of water was determined to be detrimental by introducing a small amount of water to the reactor by passing the feed gas through a bubbler. Water absorbs a substantial amount of the plasma's energy thus increasing the gases overall breakdown voltage and reducing plasma streamer stability. This instability made it difficult to get consistent results with water, which is easily demonstrated in Table 4. Note that conversion no longer obviously increases with power, and methane conversion is on average 20% lower across the board for all tests.

Table 4: Methane Conversion with Water

Watts	Alumina	CuO	CuO/MnO	CuO/ZnO
45	16%	26%	27%	14%
55	10%	20%	23%	29%
65	9%	45%	27%	44%
75	8%	64%	29%	51%

In addition to the reduced conversion, the presence of water enables the reverse water gas shift reaction for DRM and supplies an oxygen source for potential NO_x formation for methane cracking in nitrogen. (Li et al. [41]) The effects of any contaminants must be closely studied prior to development of any industrial applications.

3.6.4 Effect of pulse width

Decreasing pulse duration counterintuitively increases the average applied wattage, we're attributing this to shorter pulses favoring higher power filamentary discharges. At the typical power and reactor parameters used for this study, $1\mu\text{s}$ and $2\mu\text{s}$ pulses produce stable brush streamers while $0.5\mu\text{s}$ primarily produces sparks discharges instead. Spark discharges typically follow a more direct path and are less frequent than brush streamers which reduces the volume occupied by the plasma. This reduces its contact with the gas and would lower conversions, but this effect is counteracted by the higher energy of the sparks. Both statements can be illustrated by the NiO/CuO data in Figure 19, which shows the conversion vs wattage for different pulse widths. The first two points for NiO/CuO were taken at approximately 1700 Hz while the following three were taken at 2300 Hz. Decreasing the pulse width from $2\mu\text{s}$ to $1\mu\text{s}$ increased the applied power by about 5 watts at both frequencies, while further decreasing the width to $0.5\mu\text{s}$ increased the power by another 10 watts for the NiO/CuO. For $2\mu\text{s}$ and $1\mu\text{s}$ the conversion increases linearly with power as expected for plasma with stable brush streamers. Note that there is no difference between the slopes of the 1 and 2 μs lines, implying that they are of similar efficiency. The conversion decreases substantially for $0.5\mu\text{s}$ pulses, which can be best explained by the change in discharge type. Similar results were obtained for the ZnO/CuO catalyst with an even more drastic decrease in conversion for $0.5\mu\text{s}$ pulses.

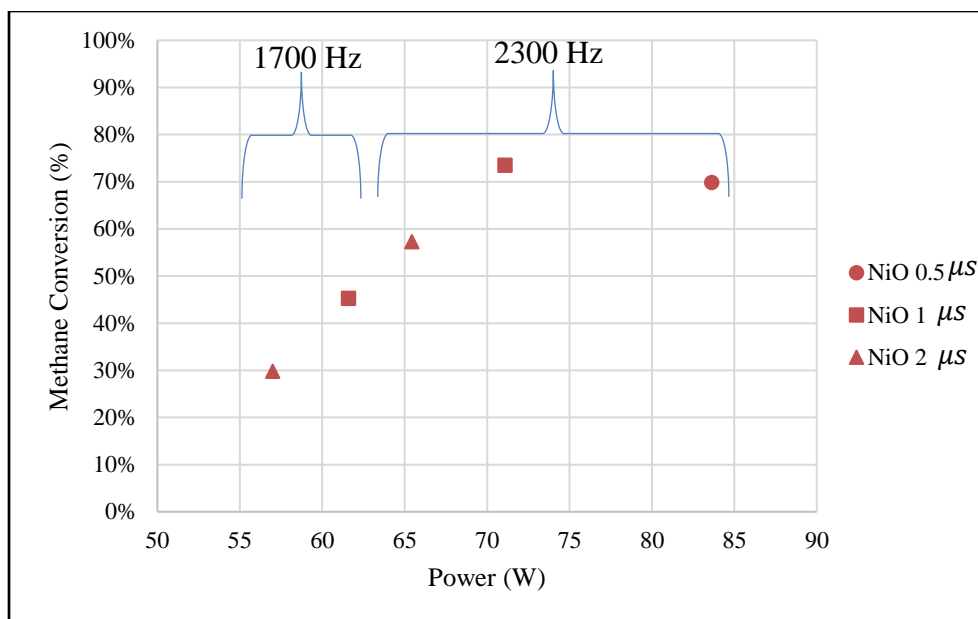


Figure 19: Conversion vs Power for Different Pulse Widths (0.5, 1, and 2 μ s)

While the spark discharges reduce the methane conversion due to its smaller active area, the higher energy density of the discharges are more likely to completely reduce the methane, which could lead in an increase in selectivity. Figure 20 shows that while there isn't an increase in hydrogen selectivity or yield, nor is there the substantial decrease in them as seen in the conversion.

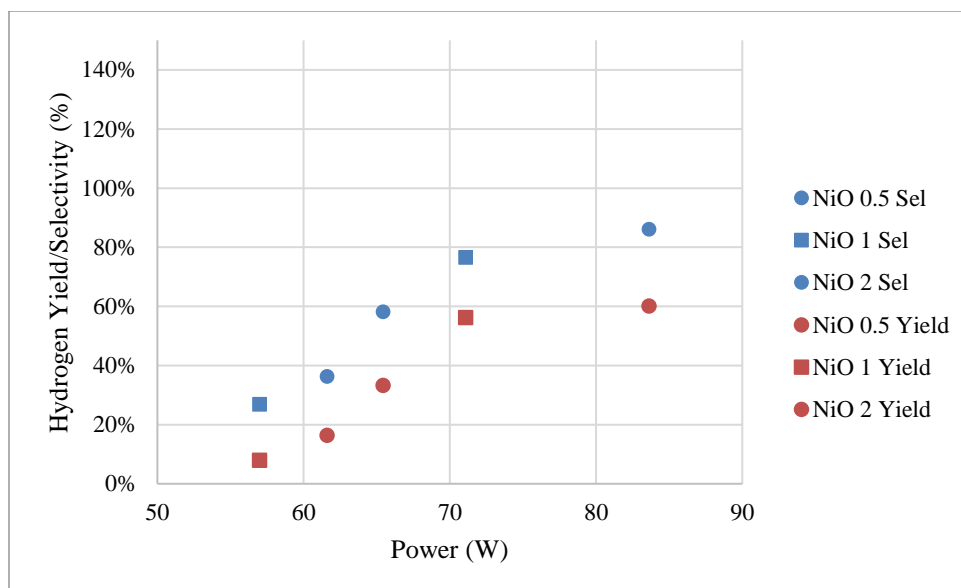


Figure 20: Selectivity & Yield vs Power for Different Pulse Widths (0.5, 1, and 2 μ s)

3.6.5 Effect of Dilution Gas

The inert carrier gas, in this case nitrogen or argon, can affect the reaction through Penning ionization and dissociation. Penning Ionization is where the inputted electrons excite the inert molecules to form ions or metastable excited states, which subsequently collide with the reagents causing ionization and dissociation of the reagents. The breakdown voltage and ionization energy of the inert affect plasma discharge type and stability in complex ways.

Nitrogen gas, while very cheap and abundant, has a rather high breakdown voltage and thus requires a high energy input to produce a stable plasma discharge. Li et al. [41] also pointed out that nitrogen gas is not completely inert and may react to form pollutants such as hydrogen cyanide and NO_x compounds. Snoeckx et al [42] determined that NO_x compounds are produced in plasma reactors in quantities that pose environmental concerns but in insignificant quantities to be utilized for nitrogen fixing.

Other inert gases could be used to lower the breakdown voltage and eliminate pollutant production. Argon and helium are the most common candidates, though other gases such as neon could theoretically be used. Table 5 shows the breakdown voltage and ionization

energy for relevant gas species. Multiple studies [43-46] show that the addition of argon increases the conversion of both CH_4 and CO_2 . Rahmani and Nikravech [43] attribute this to argon increasing the mean electron energy in the plasma. Argon does this because it is monoatomic and thus only has high energy excited states as it lacks vibrational states. This higher energy means that the excited argon is more likely to initiate an electron cascade, subsequently increasing both the number of filaments produced and the electron density. Helium has even higher energy excited states, but its small size limits collisions making electron cascades less likely, resulting in a very high mean electron energy but fewer filaments and significantly lower electron density than argon. Ozkan et al. [44] help confirm this by reporting that argon favors the production of filamentary discharges, while helium favors glow discharge. They also suggest that filamentary discharge favors CO_2 conversion while glow discharge favors methane conversion.

High percentages of inert gas will also affect product selectivity as the carbon compounds are less likely to collide with each other to form higher hydrocarbons, increasing selectivity towards the smaller molecules i.e., H_2 and CO . At high dilution percentages the energy efficiency decreases due to there being fewer molecules to react. Pinaho et al [47] reports an increase in efficiency when adding helium up to a maximum of 80% and state that there is no significant difference between argon and helium. In contrast, both Ramakers et al. [46] and Rahmani and Nikravech [43] report a roughly linear decrease in energy efficiency with increased dilution for both helium and argon. Snoeckx [42] shows that nitrogen dilution has little impact on the energy efficiency up to 50%, after which the efficiency begins to drop exponentially.

Table 5: Gas Plasma Properties

Species	Nitrogen	Helium	Argon	Carbon Dioxide	Methane
Breakdown Voltage (eV/molecule)	3.51	0.717	0.61	2.9	0.2
Ionization Energy (eV)	15.58	24.59	15.75	13.78	12.6
Lowest metastable energy (eV)	6.2	20.61	11.55	5.5	--
First Bond Dissociation Energy (eV)	9.79	--	--	5.51	4.55

In our runs with nitrogen as the diluent gas, the plasma formed a corona at lower power levels and transitioned directly into spark discharge with only a very narrow band where brush discharge occurred. When argon was used, brush discharges formed in a much broader range of parameters, and both brush and spark discharges formed at significantly lower wattages.

Methane cracking with argon is substantially more energy efficient than with nitrogen due to the production of a filamentary discharge at significantly lower power levels. Figure 21 illustrates this phenomenon by comparing methane cracking with nitrogen to one with argon over the same catalyst. The argon run yielded almost twice the methane conversion at less than half the power, resulting in an energy efficiency increase by

almost an order of magnitude. These substantial benefits will have to be weighed against the cost of separating and recovery the argon.

Significantly for our experiments, all of the DRM runs used argon as the diluent gas out of necessity, since using nitrogen interferes with our ability to detect carbon monoxide accurately using the QMS.

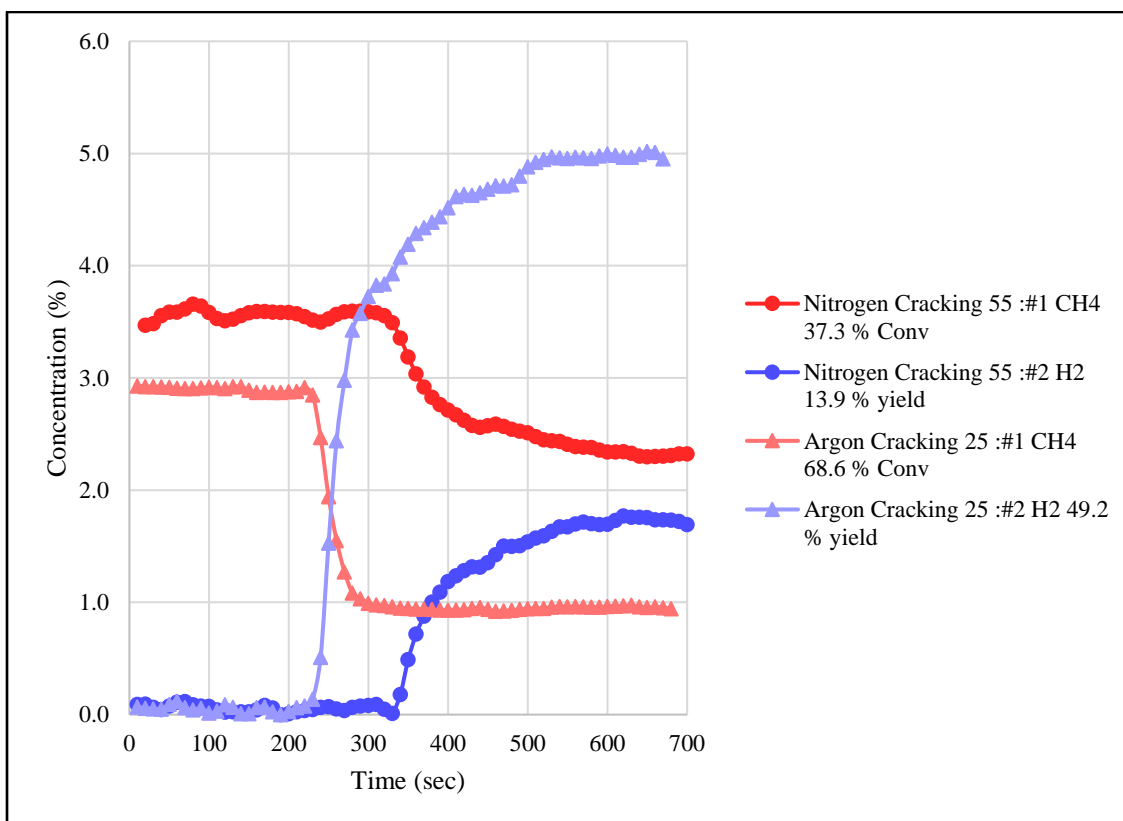


Figure 21: Nitrogen at 55 Watts vs Argon at 25 Watts

3.7 Dry Reforming of Methane

3.7.1 Effect of catalyst and plasma alone

Virtually no reaction is observed when the plasma reactor is operated without a catalyst present or when the catalyst is present and there is no plasma. This is evident since in all our tests no significant conversion of methane or carbon dioxide occurs and no products are noted until after the discharge is initiated. With a discharge and no catalyst present,

little or no reactant conversion is seen. The maximum observed conversion for methane cracking without a catalyst was 26% (at very high power) with only a 7% hydrogen yield; the low hydrogen yield suggests that the majority of this observed “conversion” is actually adsorption onto the alumina. Figure 22 shows the effect of the discharge power on a mixture of CO₂ and CH₄ without a catalyst present. At lower powers (<5 watts) no conversion of methane or carbon dioxide is seen, and the hydrogen and CO concentrations remain at their baseline values. At power level of ~10 watts some methane is consumed, and the hydrogen produced rises slightly above the baseline value. The CO concentration rises significantly above the original baseline value, and a slightly comparable decreased value for CO₂ is observed. Finally, at 26 watts, a small amount of hydrogen is seen, and there is some evidence for a low conversion level DRM reaction, but far below that seen at much lower input powers over the catalyst. This clearly demonstrates a synergistic effect between the catalyst and the plasma discharge occurs at low power inputs and that plasma activated catalysis are responsible for most of the observed activity in the DRM reactions.

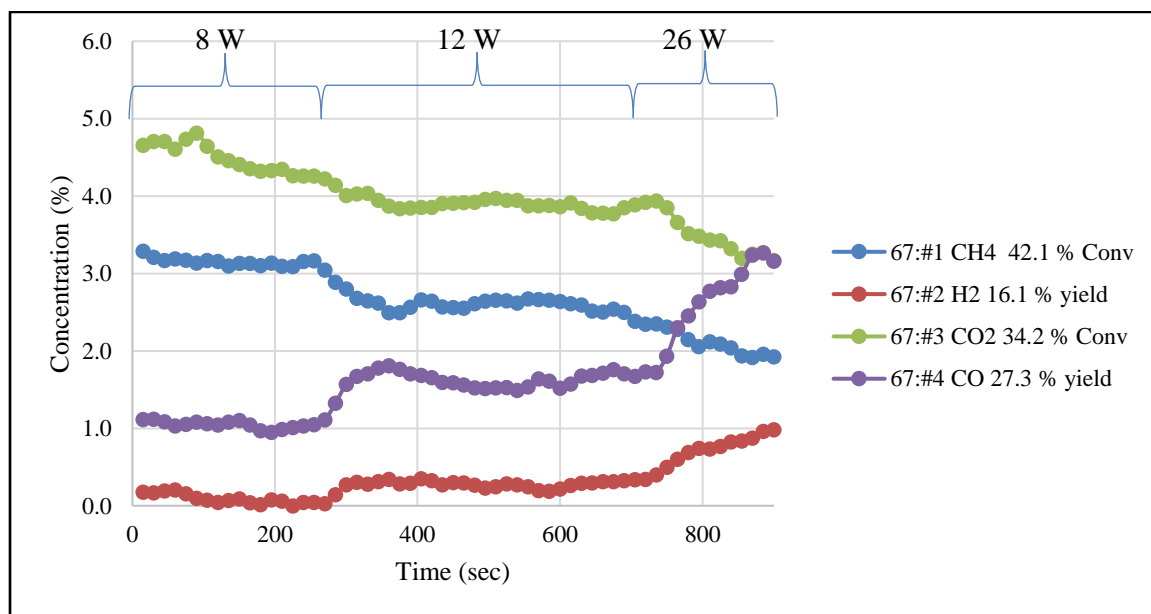


Figure 22: Three Power Levels without Catalyst

The alumina catalyst support by itself, shown in Figure 23, showed results similarly poor results to the reactor without any catalyst. In this run the alumina was not preadsorbed so the adsorption affects can be seen. The alumina support adsorbs carbon dioxide and to lesser extent methane; the extremely low yields suggest that adsorption is contributing substantially more to the loss of reagents than any actual reaction.

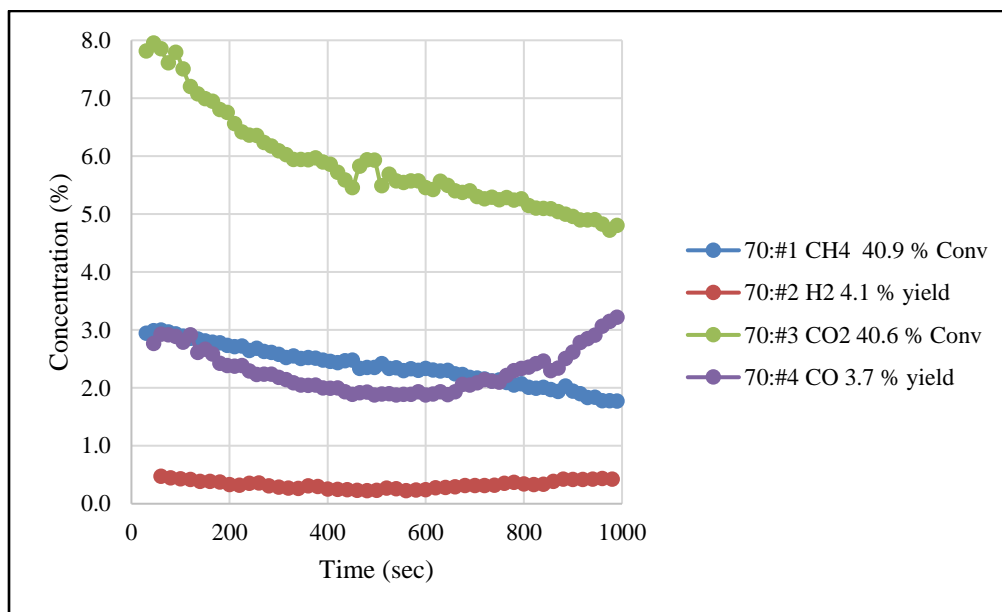


Figure 23: Alumina without Discharge

3.7.2 Effect of Catalyst Composition in DRM

When the catalyst and plasma are both present, high conversions of both methane and carbon dioxide are seen. The yields of hydrogen and carbon monoxide depend largely on the secondary metal oxide used in the catalyst, as well as the initial ratios of $\text{CO}_2:\text{CH}_4$. Examples of the effect of catalyst metals on product yields and reactant conversions are shown in the following four figures of batch reactor runs with nearly equal CO_2 and methane concentrations. In Figure 24 the alumina catalyst support with copper oxide doping is shown. The copper is in an oxidized state but consists of various forms of copper, aluminum, and oxygen. The initial pressure of carbon dioxide and methane are adjusted to be approximately the same as measured by the QMS, thus the stoichiometric ratio of reactants are also approximately the same. The absolute mole fractions of methane and carbon dioxide are both approximately 3%, with the balance of the gases being argon. The plasma discharge is initiated near 250 seconds which leads to the decline of carbon dioxide and methane in the reactor. The methane begins to decrease in the plasma discharge and simultaneously carbon monoxide and hydrogen concentrations increase in the reactor. Substantially more CO is produced than hydrogen, suggesting byproducts containing hydrogen are being formed. The most obvious candidate is water

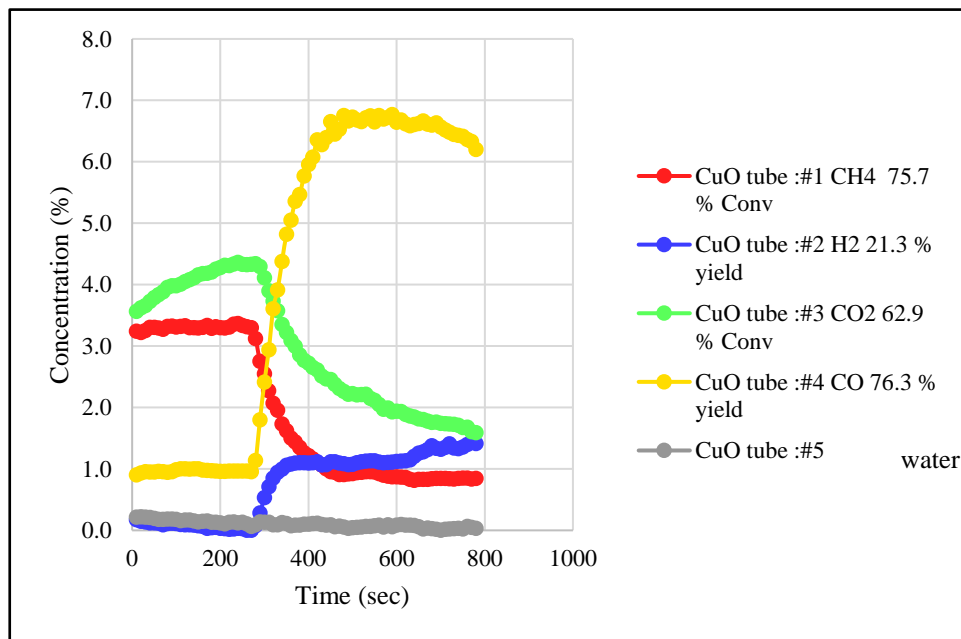


Figure 24: CuO DRM

through the water gas shift reaction (B), but the QMS shows no increase in water. The alumina in the catalyst has a very high adsorption capacity for water, enough to adsorb the maximum theoretical yield of water several times over, so it's possible that water is being produced but is entirely adsorbed onto the catalyst. The alumina also strongly adsorbs CO_2 , but in this case the effects are mitigated by pre-adsorbing it with CO_2 . The adsorption effects make it difficult to close the hydrogen mass balances with certainty. However, we are clearly seeing dry reforming of methane over the copper oxide catalyst at near ambient temperatures and pressures.

In Figure 25 we see the reaction of a near stoichiometric feed of carbon dioxide and methane over a manganese doped copper catalyst at ambient conditions. We see similar conversions and yields as we did with the plain CuO catalyst.

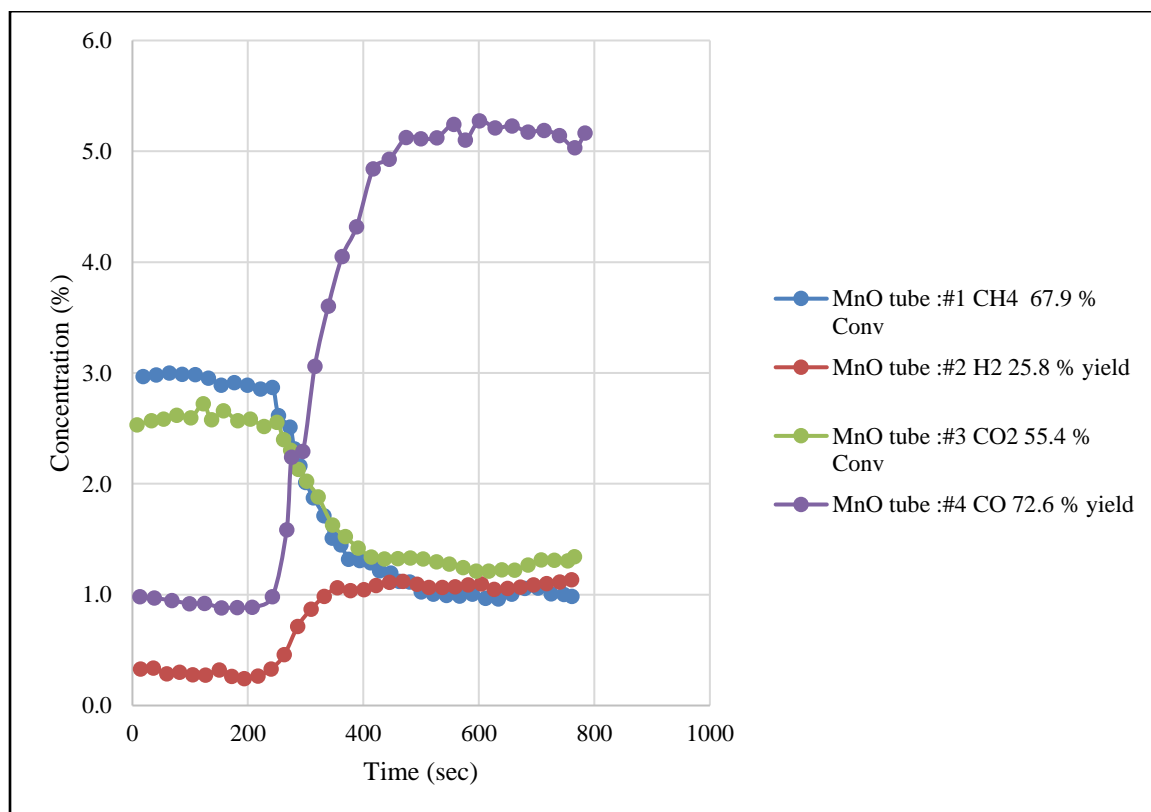


Figure 25: MnO DRM

Figure 26 also shows similar results for the reaction over a zinc copper doped catalyst, except that the hydrogen yield improves from 25.8 to 31.6%. The three catalysts all had methane conversions between 65-70%, CO₂ conversions between 55%-60%, and CO yields between 70-75%. The CuO catalyst without dopants seemed to slightly outperform the others in reactant conversion, but not for hydrogen yield.

Overall, these results are consistent with the methane activation study results, with all three catalysts achieving similar methane conversions. However, due to the use of argon as a diluent gas, all of the DRM studies had much lower input power. Taking the methane activation and DRM studies together, suggests that the activation of methane is the limiting step. The carbon monoxide selectivity for all three is close to 100%, suggesting some CO₂ pre-adsorbed on the support is also participating in the reaction. The hydrogen yield was consistently under 50%, most likely due to the reaction of hydrogen and carbon dioxide to form water, however, no significant increase in water was detected by the QMS, suggesting that any water forms remains adsorbed onto the catalyst substrate at the ambient temperatures and pressures used for the tests.

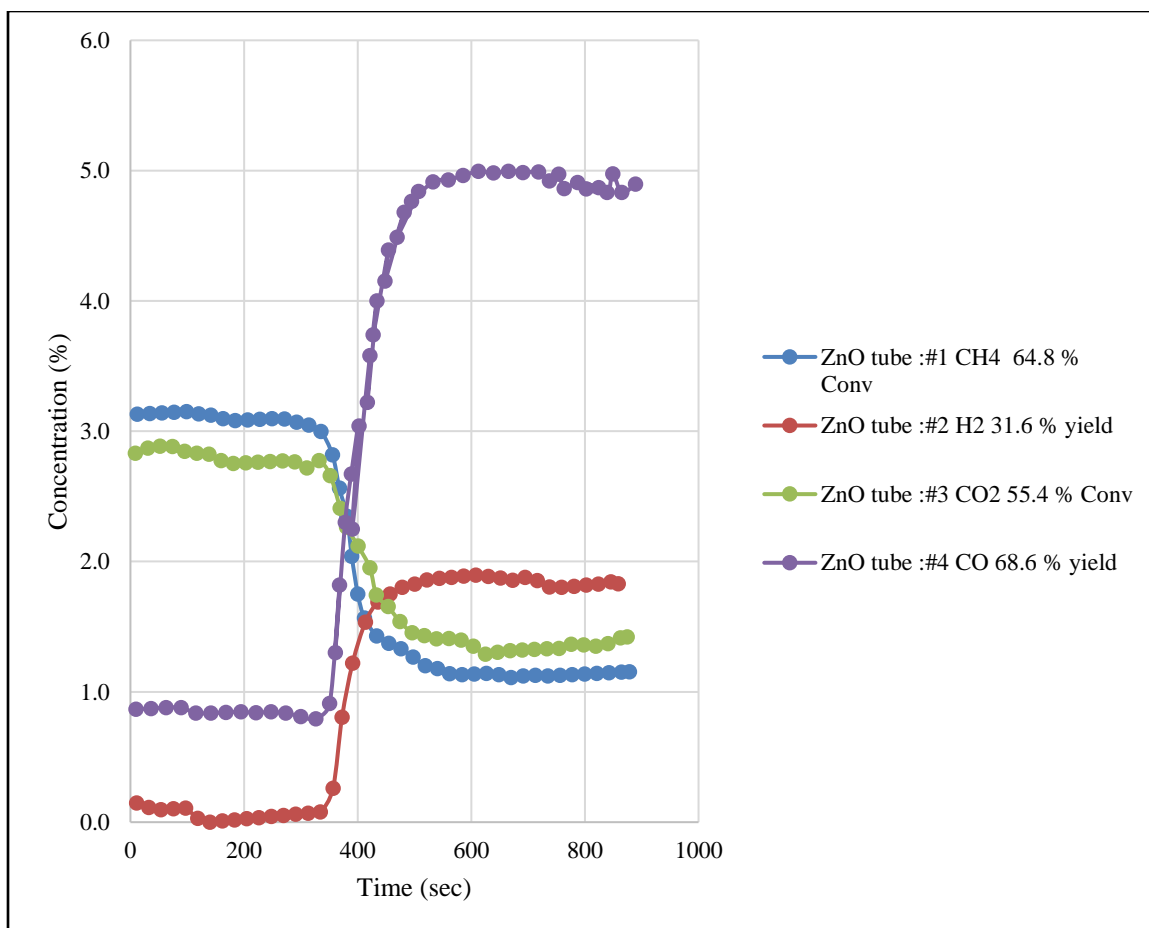


Figure 26: ZnO DRM

Finally, in Figure 27, we see a substantially different behavior for a near stoichiometric feed of carbon dioxide and methane over a copper and nickel doped catalyst. There is a more robust conversion of methane and carbon dioxide than for the other 3 catalysts, which is again in agreement with the methane cracking experiments at higher powers. The methane conversion in this case approaches 80% and the carbon dioxide conversion approaches 94%. We also see a strong initial yield of carbon monoxide, and a higher yield of hydrogen than the other catalysts. However, the carbon monoxide concentration passes through a maximum approximately 100 seconds after the plasma discharge is initiated and subsequently declines to a level almost equal to the hydrogen concentration. This is also the only catalyst composition which yielded higher hydrocarbon compounds (e.g., C₂, C₃, etc.) as observed in the QMS. Since nickel is a good catalyst for Fischer-

Tropsch reactions, the creation of higher hydrocarbons from the carbon monoxide and hydrogen is unsurprising. Therefore, the catalyst composition has an important role in the product distribution and reactant conversions and product yields for plasma assisted catalytic DRM, second only to the initial reactant ratios which have an even stronger effect.

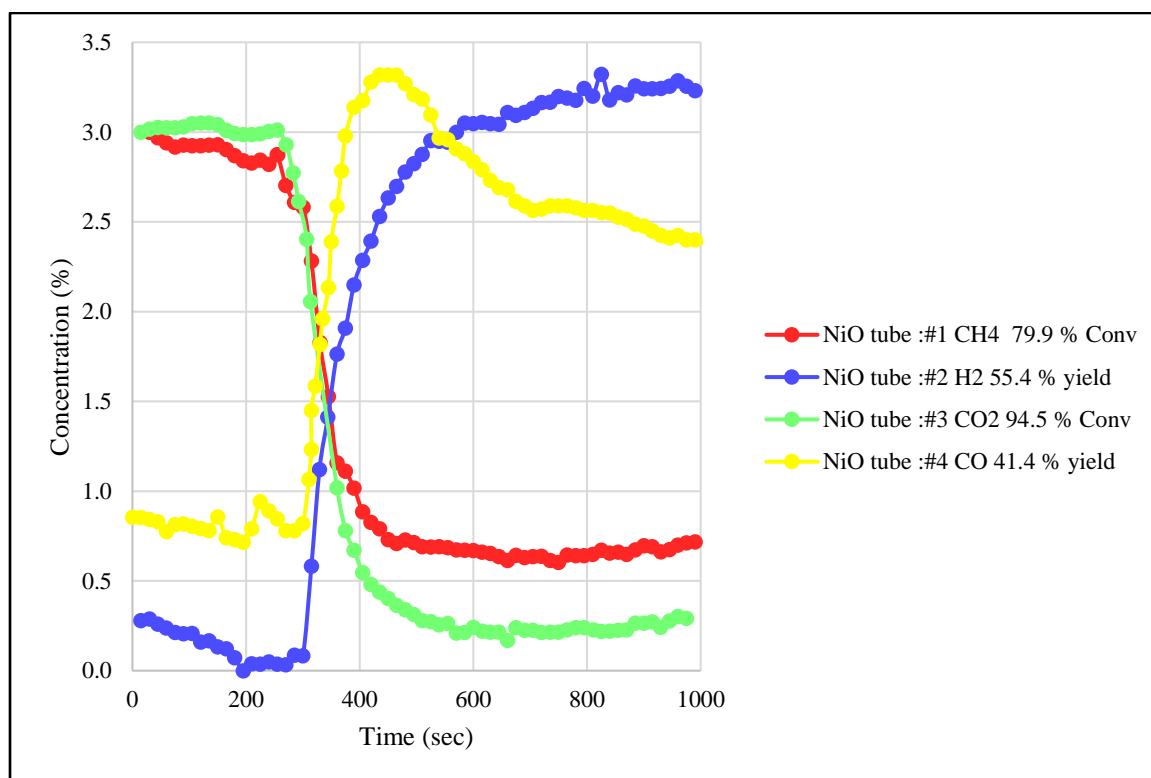


Figure 27: NiO DRM

3.7.3 Effect of Methane/CO2 ratio

We have found that the ratio of methane to carbon dioxide in the initial feed is extremely important in the reactant conversions and product yields. In figures 28, 29 and 30, plots of conversions and yields over a copper-zinc catalyst are shown for low medium and high carbon dioxide to methane ratios. The CO₂/CH₄ stoichiometric ratios are approximately 0.5/1.0, 1.0/1.0, and 1.5/1.0 respectively. Figure 28 shows the reaction of a low CO₂ to methane ratio over a copper zinc catalyst. In this case the methane conversion is slightly lower than that seen for other reactant ratios, but still close to 60%; however, the yield of

hydrogen relative to carbon monoxide is the highest at over 40%, with a ratio of hydrogen to carbon monoxide of approximately 0.8:1.0. This ratio has a lower selectivity for carbon monoxide but higher selectivity for hydrogen. This may point to a competitive surface effect, wherein lower carbon dioxide surface coverage at the low pressure ratios provides more surface access which is required for methane activation to produce hydrogen. The hydrogen pressure is also enhanced by less surface reactions involving adsorbed carbon dioxide reduction. Overall, this points to carbon dioxide as being more strongly adsorbed on the surface than methane.

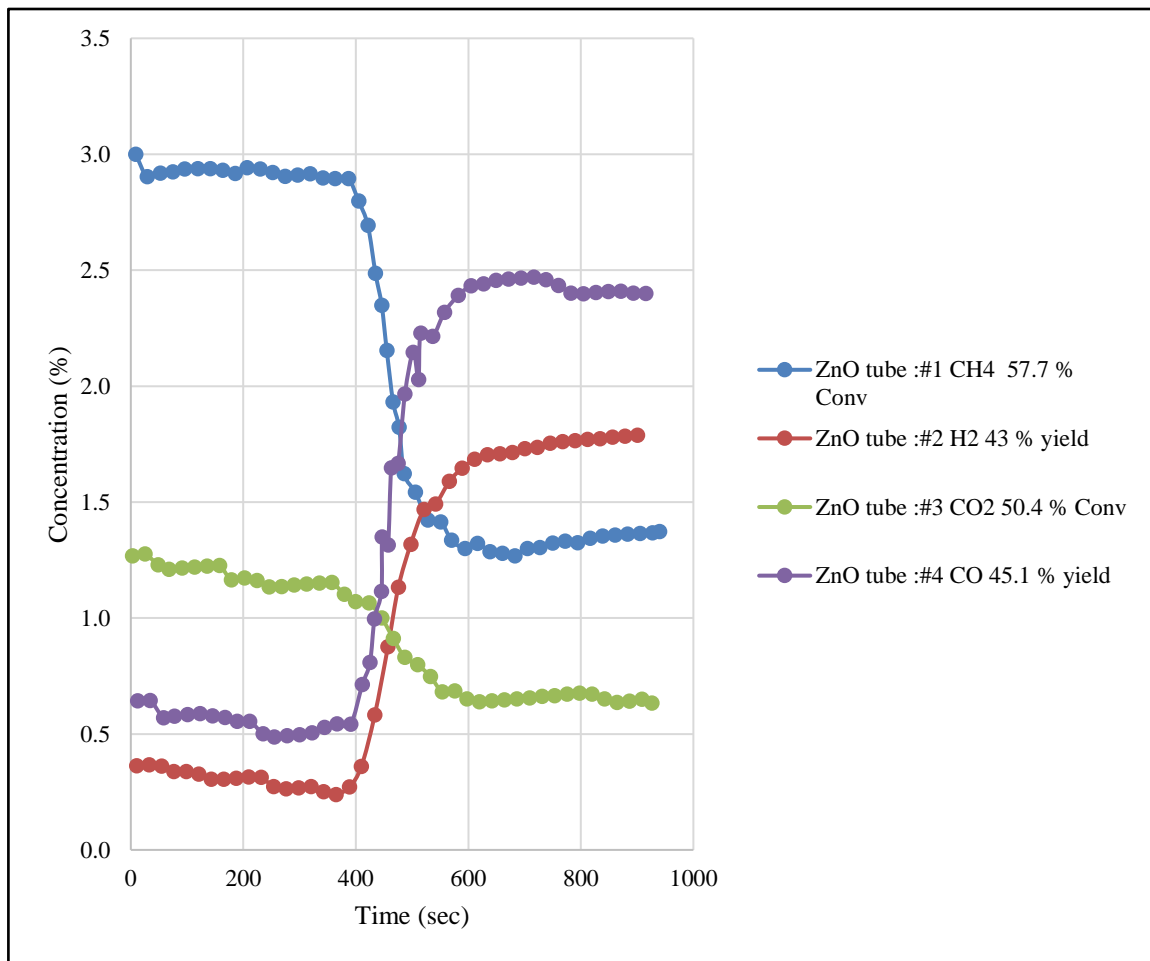


Figure 28: Low CO₂/Me ZnO DRM

Error! Reference source not found. shows an experiment with nearly equal methane to carbon dioxide ratios over the copper zinc catalyst. The results are consistent with the run shown in Figure 26, which was performed at nearly identical conditions. As compared to the low CO₂ case, there is much greater production of carbon monoxide, with yields slightly greater than would be expected based upon the carbon balance for methane and CO₂ in the gas phase alone. This again may be attributed to pre-adsorbed carbon dioxide on the catalyst surface reacting to form carbon monoxide in the presence of the active hydrogen species released from the methane. The larger concentration of carbon dioxide may also react with the free hydrogen to enhance the production of carbon monoxide. The conversions and yields are similar to those seen in the previous experiments, and the methane conversion (64%) is in the range seen in many of the experiments.

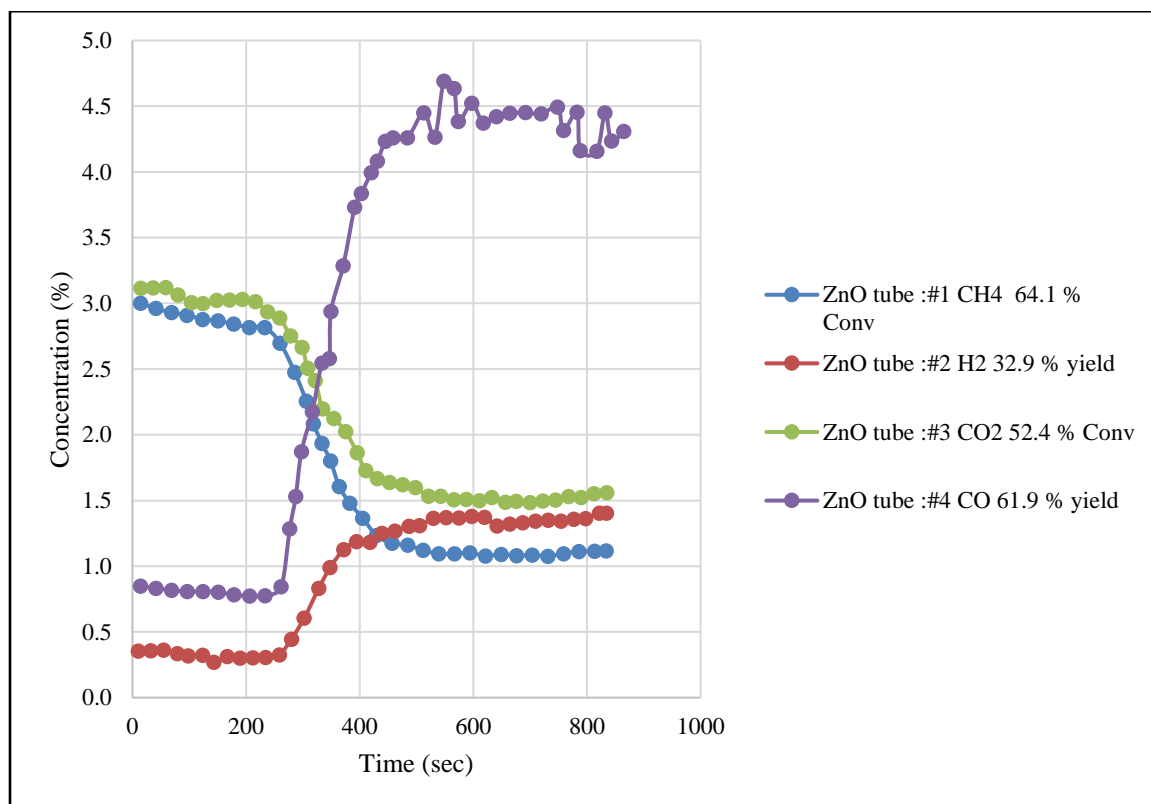


Figure 29: Equal CO₂/Me ZnO DRM

Finally, a high CO₂ to methane ratio experiment over the copper zinc catalyst is shown in Figure 30. The production of hydrogen is significantly suppressed to less than 20% yield,

and the production and yield of carbon monoxide is extremely high. This may be explained by the surface reduction of carbon dioxide by plasma phase hydrogen species to carbon monoxide and water. However, we believe that most of the water remains adsorbed onto the catalyst and is not detected by the QMS. The conversion of methane remains in the same range as the other experiments at approximately 67%. The ratio of carbon monoxide to hydrogen in this example is very high ($>10:1$), so this stoichiometry does not produce a suitable syngas mixture for further production of hydrocarbons and chemicals. Further increasing the CO_2 concentration can also negatively affect the energy efficiency, as Dubois et al. [49] found that CO_2 concentrations over 5% changes the gas's electronegativity such that higher voltages are needed to produce visible plasma. This affect was also observed in our experiments, at very high CO_2 concentrations our system is unable to provide sufficient energy to produce a visible plasma.

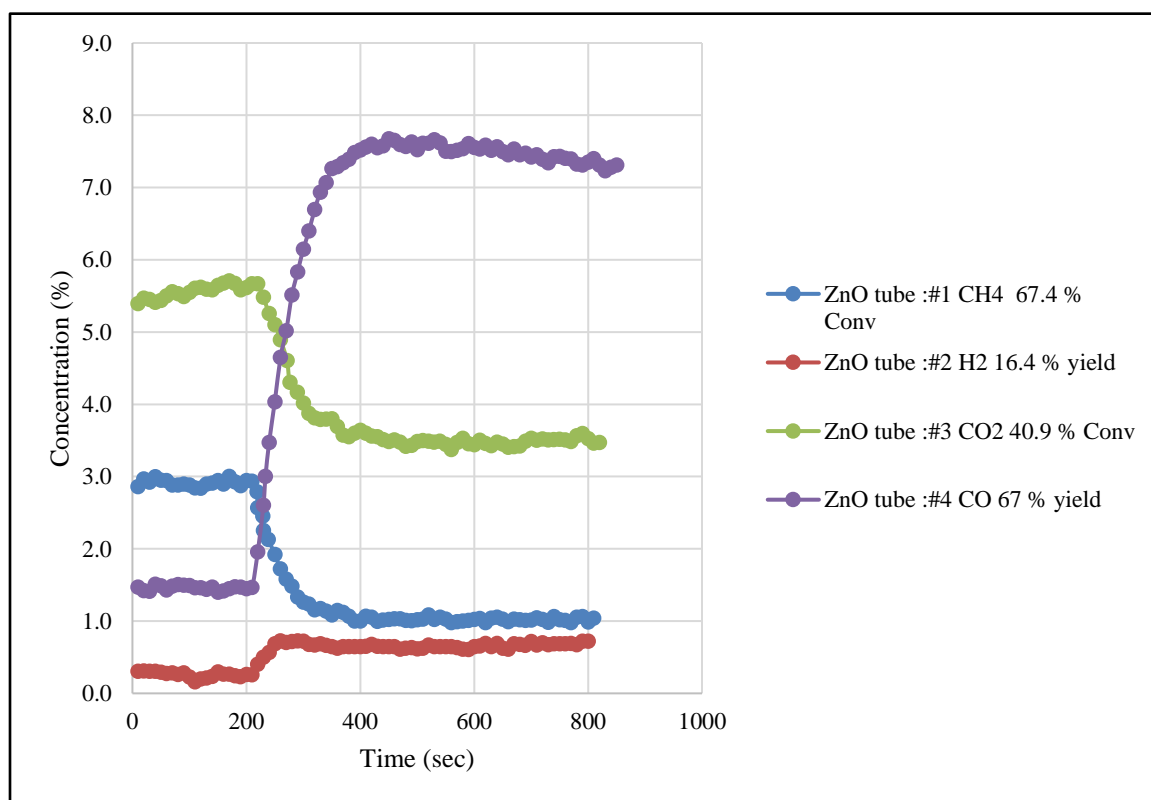


Figure 30: High CO_2/Me ZnO DRM

Overall, for the copper zinc catalyst, low carbon dioxide concentrations in the feed reactants produced the best yields for hydrogen and a more equal ratio of hydrogen to carbon monoxide. Similar tests for high medium and low ratios of reactants have been run for other catalysts in this study, and in most cases an initially high carbon dioxide concentration greatly suppress hydrogen production but enhance carbon monoxide production.

4 Discussion

4.1 Methane Activation

The activation and dissociation of methane to produce active hydrogen species is essential to the plasma DRM process. The high-energy electrons (>1 eV) generated in low-temperature pulsed plasmas induce molecule excitation, ionization, dissociation, and subsequent Penning ionization resulting in the chemical bonds breaking. Using our pulsed plasma reactor, methane in an inert carrier gas (nitrogen or argon) is readily decomposed to form hydrogen and carbon species. The bond strengths of the different hydrogens in methane as shown in Table 6.

Table 6: Methane Bond Strengths

Species	kJ/mol*	eV/Bond*
H ₃ C-H	439	4.550
H ₂ C-H	460	4.767
HC-H	423	4.384
C-H	339	3.513

These energies are readily attained in corona discharges (Zhang et al. [48]) however, other molecules in the gas phase can adsorb energy from the discharge, removing enough energy that the methane bonds are less readily activated. Therefore, we find much higher reaction rates with monoatomic argon as the inert gas than with diatomic nitrogen. In general, the pulsed corona discharge has sufficient energy to activate the hydrogen bonds in methane which dissociate at 3.5 to 4.8 eV (Table 6), but the energies are not sufficient to activate triple bonds such as found in carbon monoxide (11.6 eV) or nitrogen (9.79 eV).

The plasma discharge type and the energy imparted is the most important factor for methane activation and is the result of many experimental factors. Insufficient input energy leads to coronal (Figure 31) or an unstable streamer discharge. Significant methane activation is only obtained for stable brush streamer type (Figure 32) or with pulsed spark discharge (Figure 33). Excessive power yields continuous spark discharges with very large currents which are not as energy efficient as the filamentous brush discharge. Thus, to provide for an energy efficient reaction, the discharge must be carefully controlled to maintain the filamentous brush discharge. The addition of a catalyst changes the composition of the gas phase which contributes greatly to the discharge stability. For example, use of MnO or NiO as the catalyst or the addition of water increase the minimum energy required for stable streamer discharge. Also, the pulse duration plays a key role in that pulse widths less $1\mu\text{s}$ lead to spark discharge. The use of argon instead of nitrogen as the diluent gas also substantially lowers the power requirements for spark and streamer discharges and broadens the range for stable brush discharge. Finally, the field strength (kV/cm) is a key parameter in the gas electronic breakdown which leads to sparking. The electrode gap distance and electrode geometry chiefly determine the electric field strength, both have a significant impact on the discharge type. The solid-state pulse forming network we have developed allows for “tuning” of the system to achieve the filamentous brush discharge more effectively than mechanical or thyristor based HV systems.

The highest obtained methane conversion of 90% was obtained during an approximately 8-minute batch operating at near 40 watts on the ZnO/CuO catalyst. This run had an approximate 50% hydrogen selectivity and yield. After the catalyst was used for several experiments, the conversion dropped to near 50% for similar operating parameters. Further deactivation was not observed. This shows that the catalyst partially deactivates due to coking, but then the activity stabilizes.

The methane cracking experiments have not been optimized for energy efficiency. Typical energy conversion efficiencies in nitrogen were 1.5-3.5%. Runs with argon obtained significantly higher efficiencies 5-15%. The most efficient run was with the

plain CuO catalyst; it achieved 68% methane conversion and 84% hydrogen yield over 5 minutes at 25 watts resulting in an ECE of 15.5%.



Figure 31: Corona Discharge



Figure 32: Filamentous Brush Discharge



Figure 33: Spark Discharge over Catalyst

4.2 Role of the Catalyst in DRM

Our studies demonstrate that the alumina catalyst substrate provides a high surface area for the catalyst but does not by itself promote the dry reforming reaction. Due to the lack of DRM reaction products prior to initiating the plasma in all the catalyst experiments, it is also evident that metal oxide catalysts alone do not promote the reaction at ambient conditions. A basic goal of this study is to show that the DRM reactions are significantly promoted by the plasma in combination with the catalyst. To show this, several experiments were conducted without catalysts to determine the degree of DRM conversion using the plasma alone. Tests conducted with CH_4 and CO_2 at low power (8 watts), medium power (12 watts), and very high plasma power (26 watts) are shown in Figure 22. Our typical DRM experiments with catalysts were done at powers between 8 to 12 watts. The low, medium, and high wattages resulted in methane conversions of approximately 6%, 20%, and 40% cumulatively; far below that of even the worst plasma catalyst run (57% at 12 watts). For the catalyst plus plasma runs methane conversions varied from 57%-80% depending on the feed ratio and catalyst composition. Hence, the plasma-only decomposition reactions were probably forming carbon on the electrode surfaces. The ability of the plasma assisted catalyst system to produce large conversion of reactants and good product yields at low to moderate power inputs would indicate that the dry reforming reactions observed are due to a synergy of the plasma and catalyst

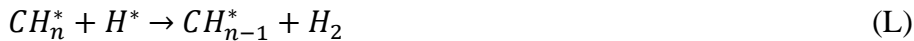
interaction. The mechanism by which this happens would therefore involve the formation and reaction of surface species. We have several experiments for the alumina catalyst support alone in which the discharge power input similarly varies, in which we observe similar results (i.e. little or no DRM reactions) which also supports the requirement that an active catalytic compound is required for the plasma enhanced catalytic DRM reaction.

Based upon the preponderance of reaction results, plus the emission studies, we believe that the reaction involves chemisorbed CO₂ on the catalyst and activated methane radicals and atomic hydrogen being generated on the surface to create CO and residual H₂ in the gas phase. Excessively high CO₂ concentrations not only absorb much of the plasma discharge energy but can also react with the hydrogen atoms to produce more CO and water as in reaction (D). Lower CO₂ concentrations still yield significant CO suggesting two mechanisms for CO production but yield much more H₂, suggesting that reactions (C) and (D) both occur and the dominant one is determined by the feed ratio.



4.3 Evidence for Reaction Mechanism based on Reactant Ratios

In methane activation, the high conversion is only observed in the presence of a catalyst, which suggests a surface catalyzed reaction. It's unclear if the reaction is primarily taking place on the catalyst (H & I) or they just produced the ions necessary to start a chain reaction through reactions (K & L). Fresh catalyst runs had very high methane conversion and hydrogen selectivity, however they quickly partially deactivated. This could imply the most active catalyst sites are converting methane directly to hydrogen through reaction H, but quickly become deactivated due to the solid carbon being produced on the catalyst surface. The less active sites only activate the methane via reaction I, with further hydrogen production taking place in the gas phase through various means (reaction J-L).



In DRM, methane conversion increases slightly with increased CO₂ feed, but is lower than when reacting methane alone.. This suggests that the majority of methane is not converted on the catalyst surface (H & I), as the added CO₂ would be competing for catalyst sites. The coking trends further support this. The increase in methane conversion is logical as methane and methyl radicals can now react through pathway M as well as the aforementioned pathways.





Hydrogen production is substantially reduced for high CO₂/CH₄ ratios. This suggests that hydrogen is being consumed through reaction N. At higher ratios the majority of catalyst active sites will be filled with CO₂ preventing methane from adsorption onto the catalyst. This leads to reaction N being favored over reaction M. Additionally, excess CO₂ will push the equilibrium of reaction N towards water.

Surprisingly no increase in water was detected by the QMS. The alumina catalyst support has a very high adsorption capacity for water, several times the amount that is theoretically being produced based on the hydrogen balance, which could partially explain the absence of water, but further studies are needed to verify the mechanisms.

5 Conclusions

We have developed and demonstrated a novel pulsed-plasma catalytic DRM reactor that obtains high conversion of reactants and excellent yields of both hydrogen and carbon monoxide. A solid state HV pulse generator was developed which allows for fine tuning of pulse shape, rise times, duration, and frequency, and thus is a substantial improvement over older pulse generating circuits. It generates a positive nano-second pulsed corona/streamer discharge at atmospheric pressure and near ambient temperature, giving it a significant advantage in practicality over radio frequency, microwave, and glow discharge plasma systems. A series of copper-oxide catalysts doped with either MnO, ZnO, or NiO were synthesized specifically for plasma DRM. The catalysts were successfully coupled to the excited state plasma in situ using our novel reactor design. A series of tests were conducted to determine the catalysts' performance both for DRM and for cracking methane by itself. A residual gas analyzer and emission spectrophotometer were used to collect live reaction data, allowing for substantially more data to be analyzed than with traditional methods such as GCMS. All the catalysts showed substantial improvement over the control, but their performance degraded over time due to coking.

Methane conversions up to 90% and hydrogen yields up to 85% were obtained with fresh catalyst for the methane activation studies. However, energy efficiency were quite low 1.5-3.5%; efficiency could be improved to 5-15% by using argon instead of nitrogen as the carrier gas. The MnO and ZnO doped catalysts performed similarly to the copper catalyst without dopants. The NiO doped catalyst outperformed the other catalysts at high power inputs. The plasma type (corona, streamer, or spark) was found to be of great importance to methane cracking, with significant conversion only being obtained for streamer and spark discharge.

The methane cracking catalyst results were found to be indicative of the DRM catalyst results. In DRM, the NiO doped greatly outperformed the other catalysts in all metrics and was the only catalyst that produced detectable quantities of higher hydrocarbons.

Methane and carbon dioxide conversions of up to 80% and 95% were obtained respectively with hydrogen and carbon monoxide yields of up to 50% and 40%. The feed ratio was found to be of great importance for DRM with the best results at a 1:1 ratio of CO_2 to CH_4 . High CO_2/CH_4 ratios led to very low hydrogen yields. The energy conversion efficiency varied greatly between runs, the highest obtained in batch mode was 25%. Flow reactors will be more efficient than batch ones; a preliminary flow mode test resulted in an ECE of 55%. For comparison, electrolysis of water has an ECE around 75%. While optimization would further improve the efficiency, factors such as argon recovery were not accounted for in the efficiency calculations.

In conclusion, we've shown that:

- Our pulsed plasma reactor enables both methane cracking and DRM with high conversions and yields at near ambient temperatures and pressures.
- Significant conversion is only obtained when the plasma is combined with a catalyst.
- The plasma type is important for methane activation, significant conversion is only obtained for brush and spark discharges.
- Using argon as the carrier gas instead of nitrogen causes a substantial increase in energy efficiency.
- The NiO/CuO catalyst greatly outperforms the other catalysts in DRM, and was the only catalyst to produce higher hydrocarbons.
- DRM product distribution can be controlled by the feed ratio.

6 Recommendations

The proposed technology is transformational in that it is an alternative to traditional thermal and catalytic reactions for important gas phase reaction chemistries. Since the energy from the pulsed electrical discharge goes primarily into the electronic states associated with the molecules and not into thermal modes, reactions previously only possible at high temperatures and severe reaction conditions might be carried out at near ambient temperatures and pressures. The new technology opens the door to non-thermal chemical pathways that are potentially much more energy efficient, carbon neutral, can be used for hydrogen production, and employ a variety of important green chemistry not normally achievable via thermal or traditional catalytic routes.

While the effectiveness of this system exceeded expectations, it is still only a proof of concept, there are several areas that need further investigations before plasma DRM can be considered for real applications.

- Batch mode experiments introduced transient affects that made accurate concentration measurements difficult. With the basic kinetics better understood, a small pilot-scale flow reactor with greater power input and gas-phase throughput should be investigated.
- The catalyst coking effects need to be studied in a longer duration study.
- The plasma properties should be investigated to better understand the reaction mechanism and will be important for optimization. Murray describes various methods for determining plasma and electron properties based on laser scattering [50]. A similar approach could be employed here.
- The solid-state pulse producing network allows us to finely tune the pulse characteristics, the optimal parameters should be determined.
- Once the efficiency of an optimized system is known, an economic analysis should be performed to evaluate the viability of plasmas DRM for syngas production.

- Further analysis of DRM products would be helpful. Using NiO/CuO higher hydrocarbon peaks were detected but the species were not identified. Additionally, there is a low hydrogen selectivity for high CO₂/CH₄ ratios; we've presumed that water formation is the cause of this, but confirmation is needed.
- Further characterization of the excited state species and understanding how they couple to the catalyst need to be a focus of future studies.
- A Life Cycle Assessment (LCA) should be completed to compare the proposed DRM process to existing and other proposed methods for hydrogen production.

7 Reference List

1. *Hydrogen Production: Natural Gas Reforming*. (n.d.). Energy.Gov. Retrieved June 27, 2022, from <https://www.energy.gov/eere/fuelcells/hydrogen-production-natural-gas-reforming>
2. Perathoner, S., & Centi, G. (2014). CO₂ Recycling: A Key Strategy to Introduce Green Energy in the Chemical Production Chain. *ChemSusChem*, 7(5), 1274–1282. <https://doi.org/10.1002/cssc.201300926>
3. Shaobin Wang, G. Q. (Max) Lu and Graeme J. Millar. (1996) Carbon Dioxide Reforming of Methane to Produce Synthesis Gas over Metal-Supported Catalysts: State of the Art Energy Fuels, 10, 4, 896–904
4. Pakhare, D. and Spivey, J. (2014). A review of dry (CO₂) reforming of methane over noble metal catalysts. *Chem. Soc. Rev.*, 43, 7813–7837
5. Lavoie, J. M. (2014). Review on dry reforming of methane, a potentially more environmentally-friendly approach to the increasing natural gas exploitation. *Frontiers in Chemistry*, 2. <https://doi.org/10.3389/fchem.2014.00081>
6. le Saché, E., & Reina, T. (2022). Analysis of Dry Reforming as direct route for gas phase CO₂ conversion. The past, the present and future of catalytic DRM technologies. *Progress in Energy and Combustion Science*, 89, 100970. <https://doi.org/10.1016/j.pecs.2021.100970>
7. Bogaerts, A., & Centi, G. (2020). Plasma Technology for CO₂ Conversion: A Personal Perspective on Prospects and Gaps. *Frontiers in Energy Research*, 8. <https://doi.org/10.3389/fenrg.2020.00111>
8. Snoeckx, R., & Bogaerts, A. (2017). Plasma technology – a novel solution for CO₂ conversion? *Chemical Society Reviews*, 46(19), 5805–5863. <https://doi.org/10.1039/c6cs00066e>
9. Seyed-Matin, N., Jalili, A. H., Jenab, M. H., Zekordi, S. M., Afzali, A., Rasouli, C., & Zamaniyan, A. (2010). DC-Pulsed Plasma for Dry Reforming of Methane to Synthesis Gas. *Plasma Chemistry and Plasma Processing*, 30(3), 333–347. <https://doi.org/10.1007/s11090-010-9225-8>

10. Bak, M. S., Im, S. K., & Cappelli, M. (2015). Nanosecond-pulsed discharge plasma splitting of carbon dioxide. *IEEE Transactions on Plasma Science*, 43(4), 1002–1007. <https://doi.org/10.1109/tps.2015.2408344>
11. Sekine, Y., Yamadera, J., Matsukata, M., & Kikuchi, E. (2010). Simultaneous dry reforming and desulfurization of biomethane with non-equilibrium electric discharge at ambient temperature. *Chemical Engineering Science*, 65(1), 487–491. <https://doi.org/10.1016/j.ces.2009.06.011>
12. Cheng, H., Fan, J., Zhang, Y., Liu, D., & Ostrikov, K. K. (2020). Nanosecond pulse plasma dry reforming of natural gas. *Catalysis Today*, 351, 103–112. <https://doi.org/10.1016/j.cattod.2018.11.026>
13. Zhao, Y., Pan, Y. X., Xie, Y., & Liu, C. J. (2008). Carbon dioxide reforming of methane over glow discharge plasma-reduced Ir/Al₂O₃ catalyst. *Catalysis Communications*, 9(7), 1558–1562. <https://doi.org/10.1016/j.catcom.2007.12.024>
14. Mei, D., Liu, S., & Tu, X. (2017). CO₂ reforming with methane for syngas production using a dielectric barrier discharge plasma coupled with Ni/γ-Al₂O₃ catalysts: Process optimization through response surface methodology. *Journal of CO₂ Utilization*, 21, 314–326. <https://doi.org/10.1016/j.jcou.2017.06.020>
15. Mei, D., Zhang, P., Duan, G., Liu, S., Zhou, Y., Fang, Z., & Tu, X. (2022). CH₄ reforming with CO₂ using a nanosecond pulsed dielectric barrier discharge plasma. *Journal of CO₂ Utilization*, 62, 102073. <https://doi.org/10.1016/j.jcou.2022.102073>
16. Kuznetsov, D. L., Uvarin, V. V., & Filatov, I. E. (2021). Conversion of Methane in Plasma of Pulsed Nanosecond Discharges. *IEEE Transactions on Plasma Science*, 49(9), 2604–2612. <https://doi.org/10.1109/tps.2021.3075101>
17. Sun, H., Zhang, S., Gao, Y., Huang, B., Zhang, C., & Shao, T. (2019). Non-oxidative methane conversion in diffuse, filamentary, and spark regimes of nanosecond repetitively pulsed discharge with negative polarity. *Plasma Processes and Polymers*, 16(8), 1900050. <https://doi.org/10.1002/ppap.201900050>

18. Abiev, R. S., Sladkovskiy, D. A., Semikin, K. V., Murzin, D. Y., & Rebrov, E. V. (2020). Non-Thermal Plasma for Process and Energy Intensification in Dry Reforming of Methane. *Catalysts*, 10(11), 1358.
<https://doi.org/10.3390/catal10111358>
19. Andersen, J., Christensen, J., Østberg, M., Bogaerts, A., & Jensen, A. (2020). Plasma-catalytic dry reforming of methane: Screening of catalytic materials in a coaxial packed-bed DBD reactor. *Chemical Engineering Journal*, 397, 125519.
<https://doi.org/10.1016/j.cej.2020.125519>
20. Brune, L., Ozkan, A., Genty, E., Visart De Bocarmé, T., & Reniers, F. (2018). Dry reforming of methane via plasma-catalysis: influence of the catalyst nature supported on alumina in a packed-bed DBD configuration. *Journal of Physics D: Applied Physics*, 51(23), 234002. <https://doi.org/10.1088/1361-6463/aac047>
21. Tu, X., & Whitehead, J. (2012). Plasma-catalytic dry reforming of methane in an atmospheric dielectric barrier discharge: Understanding the synergistic effect at low temperature. *Applied Catalysis B: Environmental*, 125, 439–448.
<https://doi.org/10.1016/j.apcatb.2012.06.006>
22. Zhang, A. J., Zhu, A. M., Guo, J., Xu, Y., & Shi, C. (2010). Conversion of greenhouse gases into syngas via combined effects of discharge activation and catalysis. *Chemical Engineering Journal*, 156(3), 601–606.
<https://doi.org/10.1016/j.cej.2009.04.069>
23. Wang, H., Han, J., Bo, Z., Qin, L., Wang, Y., & Yu, F. (2019). Non-thermal plasma enhanced dry reforming of CH₄ with CO₂ over activated carbon supported Ni catalysts. *Molecular Catalysis*, 475, 110486.
<https://doi.org/10.1016/j.mcat.2019.110486>
24. Gao, X., Lin, Z., Li, T., Huang, L., Zhang, J., Askari, S., Dewangan, N., Jangam, A., & Kawi, S. (2021). Recent Developments in Dielectric Barrier Discharge Plasma-Assisted Catalytic Dry Reforming of Methane over Ni-Based Catalysts. *Catalysts*, 11(4), 455. <https://doi.org/10.3390/catal11040455>
25. Lu, N., Bao, X., Jiang, N., Shang, K., Li, J., & Wu, Y. (2017). Non-Thermal Plasma-Assisted Catalytic Dry Reforming of Methane and Carbon Dioxide Over

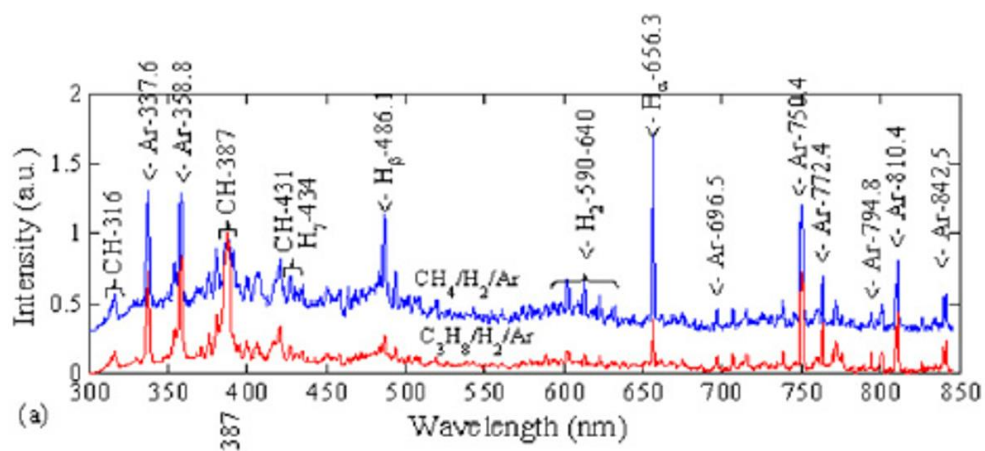
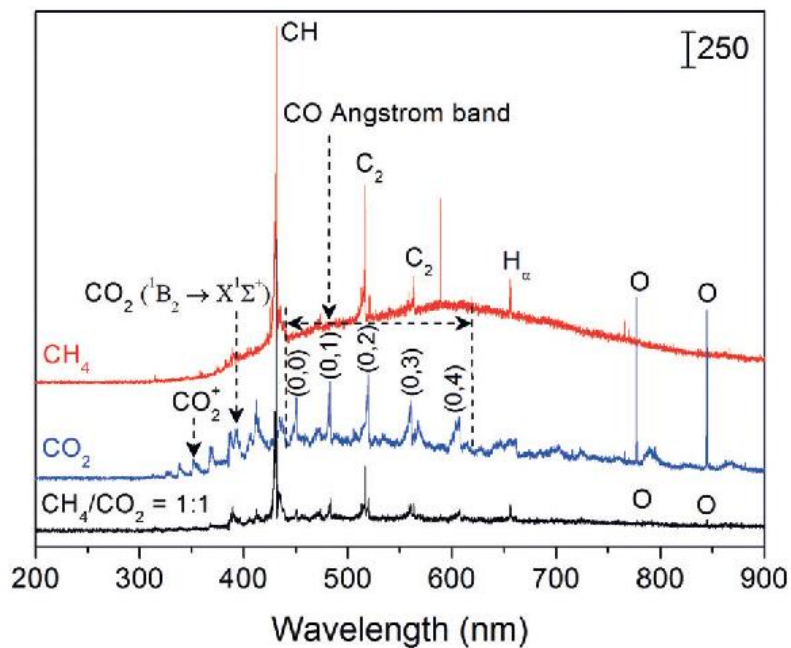
- G-C₃N₄-Based Catalyst. *Topics in Catalysis*, 60(12–14), 855–868.
<https://doi.org/10.1007/s11244-017-0750-z>
26. Xu, S., Chen, H., Hardacre, C., & Fan, X. (2021). Non-thermal plasma catalysis for CO₂ conversion and catalyst design for the process. *Journal of Physics D: Applied Physics*, 54(23), 233001. <https://doi.org/10.1088/1361-6463/abe9e1>
 27. Dėbek, R., Azzolina-Jury, F., Travert, A., & Maugé, F. (2019). A review on plasma-catalytic methanation of carbon dioxide – Looking for an efficient catalyst. *Renewable and Sustainable Energy Reviews*, 116, 109427.
<https://doi.org/10.1016/j.rser.2019.109427>
 28. Puliyalil, H., Lašič Jurković, D., Dasireddy, V. D. B. C., & Likozar, B. (2018). A review of plasma-assisted catalytic conversion of gaseous carbon dioxide and methane into value-added platform chemicals and fuels. *RSC Advances*, 8(48), 27481–27508. <https://doi.org/10.1039/c8ra03146k>
 29. Eliasson, B., Kogelschatz, U., Xue, B., & Zhou, L. M. (1998). Hydrogenation of Carbon Dioxide to Methanol with a Discharge-Activated Catalyst. *Industrial & Engineering Chemistry Research*, 37(8), 3350–3357.
<https://doi.org/10.1021/ie9709401>
 30. Gao, P., Li, F., Xiao, F., Zhao, N., Wei, W., Zhong, L., & Sun, Y. (2012). Effect of hydrotalcite-containing precursors on the performance of Cu/Zn/Al/Zr catalysts for CO₂ hydrogenation: Introduction of Cu²⁺ at different formation stages of precursors. *Catalysis Today*, 194(1), 9–15.
<https://doi.org/10.1016/j.cattod.2012.06.012>
 31. Song, H. K., Lee, H., Choi, J. W., & Na, B. K. (2004). Effect of Electrical Pulse Forms on the CO₂ Reforming of Methane Using Atmospheric Dielectric Barrier Discharge. *Plasma Chemistry and Plasma Processing*, 24(1), 57–72.
<https://doi.org/10.1023/b:pcpp.00000004882.33117.42>
 32. Isahak, W. N. R. W., Ramli, Z. A. C., Ismail, M. W., Ismail, K., Yusop, R. M., Hisham, M. W. M., & Yarmo, M. A. (2013). Adsorption–desorption of CO₂ on different type of copper oxides surfaces: Physical and chemical attractions

- studies. *Journal of CO₂ Utilization*, 2, 8–15.
<https://doi.org/10.1016/j.jcou.2013.06.002>
33. Chung, W. C., & Chang, M. B. (2016b, September). Dry reforming of methane by combined spark discharge with a ferroelectric. *Energy Conversion and Management*, 124, 305–314. <https://doi.org/10.1016/j.enconman.2016.07.023>
 34. Sheng, Z., Watanabe, Y., Kim, H. H., Yao, S., & Nozaki, T. (2020). Plasma-enabled mode-selective activation of CH₄ for dry reforming: First touch on the kinetic analysis. *Chemical Engineering Journal*, 399, 125751.
<https://doi.org/10.1016/j.cej.2020.125751>
 35. Berthelot, A., & Bogaerts, A. (2017). Modeling of CO₂ Splitting in a Microwave Plasma: How to Improve the Conversion and Energy Efficiency. *The Journal of Physical Chemistry C*, 121(15), 8236–8251.
<https://doi.org/10.1021/acs.jpcc.6b12840>
 36. Shao, T., Wang, R., Zhang, C., & Yan, P. (2018). Atmospheric-pressure pulsed discharges and plasmas: mechanism, characteristics and applications. *High Voltage*, 3(1), 14–20. <https://doi.org/10.1049/hve.2016.0014>
 37. Scapinello, M., Martini, L. M., Dilecce, G., & Tosi, P. (2016). Conversion of CH₄/CO₂ by a nanosecond repetitively pulsed discharge. *Journal of Physics D: Applied Physics*, 49(7), 075602. <https://doi.org/10.1088/0022-3727/49/7/075602>
 38. Sentek, J., Krawczyk, K., Młotek, M., Kalczewska, M., Kroker, T., Kolb, T., Schenk, A., Gericke, K. H., & Schmidt-Szałowski, K. (2010). Plasma-catalytic methane conversion with carbon dioxide in dielectric barrier discharges. *Applied Catalysis B: Environmental*, 94(1–2), 19–26.
<https://doi.org/10.1016/j.apcatb.2009.10.016>
 39. Lim, C.H. (2011) Production of Liquid Core-Polymer Shell Microcapsules. Ph.D. Dissertation, Michigan Technological University.
 40. Wang, X., Gao, Y., Zhang, S., Sun, H., Li, J., & Shao, T. (2019). Nanosecond pulsed plasma assisted dry reforming of CH₄: The effect of plasma operating

- parameters. *Applied Energy*, 243, 132–144.
<https://doi.org/10.1016/j.apenergy.2019.03.193>
41. Li, J., Yao, S., & Wu, Z. (2020). NO_x production in plasma reactors by pulsed spark discharges. *Journal of Physics D: Applied Physics*, 53(38), 385201.
<https://doi.org/10.1088/1361-6463/ab946a>
 42. Snoeckx, R., Heijckers, S., van Wesenbeeck, K., Lenaerts, S., & Bogaerts, A. (2016). CO₂ conversion in a dielectric barrier discharge plasma: N₂ in the mix as a helping hand or problematic impurity? *Energy & Environmental Science*, 9(3), 999–1011. <https://doi.org/10.1039/c5ee03304g>
 43. Rahmani, A., & Nikravech, M. (2018). Impact of Argon in Reforming of (CH₄ + CO₂) in Surface Dielectric Barrier Discharge Reactor to Produce Syngas and Liquid Fuels. *Plasma Chemistry and Plasma Processing*, 38(3), 517–534.
<https://doi.org/10.1007/s11090-018-9886-2>
 44. Ozkan, A., Dufour, T., Arnoult, G., de Keyzer, P., Bogaerts, A., & Reniers, F. (2015). CO₂–CH₄ conversion and syngas formation at atmospheric pressure using a multi-electrode dielectric barrier discharge. *Journal of CO₂ Utilization*, 9, 74–81. <https://doi.org/10.1016/j.jcou.2015.01.002>
 45. Zeng, Y., & Tu, X. (2017). Plasma-catalytic hydrogenation of CO₂ for the cogeneration of CO and CH₄ in a dielectric barrier discharge reactor: effect of argon addition. *Journal of Physics D: Applied Physics*, 50(18), 184004.
<https://doi.org/10.1088/1361-6463/aa64bb>
 46. Ramakers, M., Michiels, I., Aerts, R., Meynen, V., & Bogaerts, A. (2015). Effect of Argon or Helium on the CO₂ Conversion in a Dielectric Barrier Discharge. *Plasma Processes and Polymers*, 12(8), 755–763.
<https://doi.org/10.1002/ppap.201400213>
 47. Pinhão, N. R., Janeco, A., & Branco, J. B. (2011). Influence of Helium on the Conversion of Methane and Carbon dioxide in a Dielectric Barrier Discharge. *Plasma Chemistry and Plasma Processing*, 31(3), 427–439.
<https://doi.org/10.1007/s11090-011-9294-3>

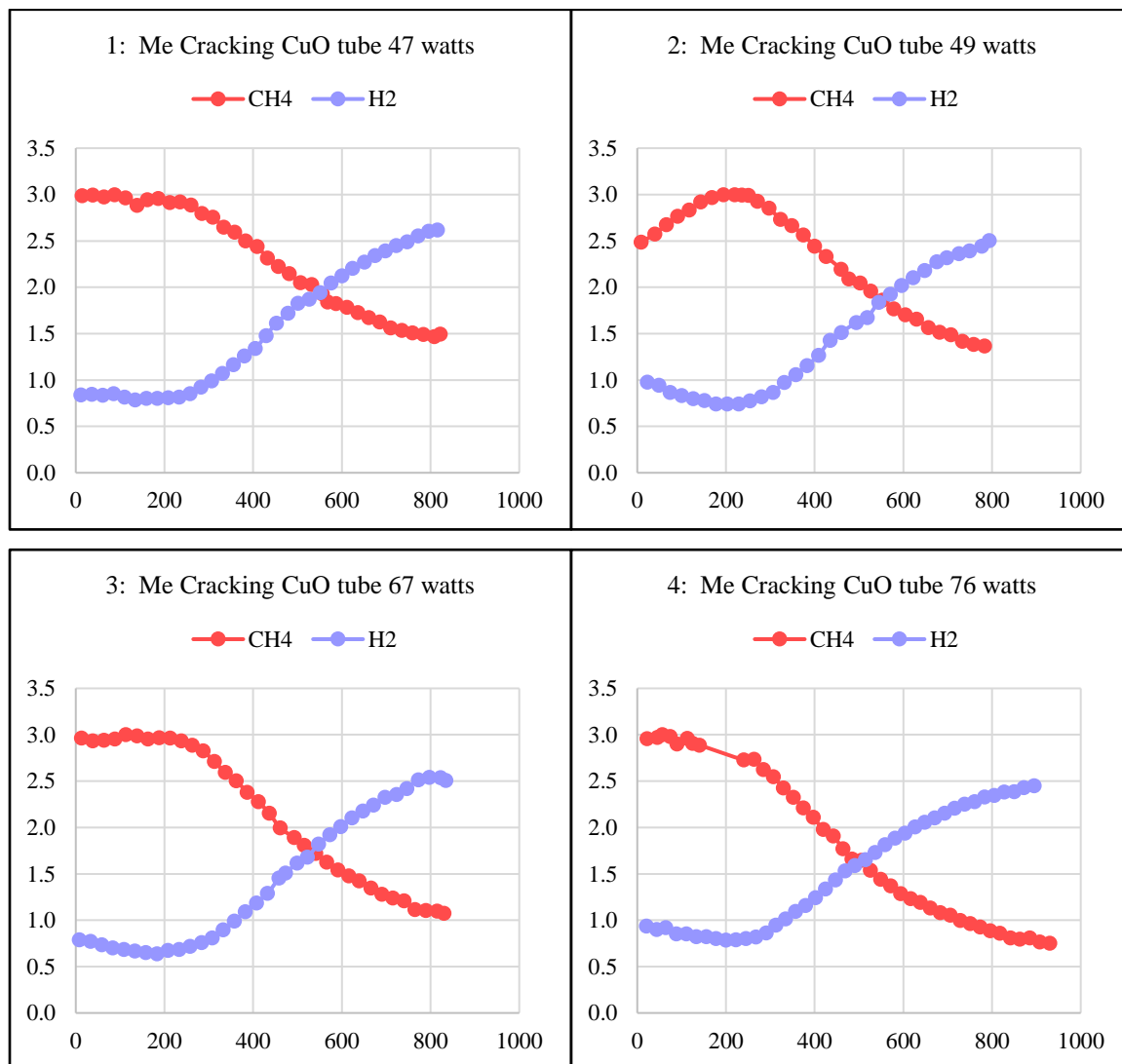
48. Zhang, Cheng & Wang, Ruixue & Yan, Ping & Shao, Tao. (2016). Atmospheric-Pressure Pulsed Discharges and Plasmas: Mechanism, Characteristics and Applications. High Voltage. 3. 10.1049/hve.2016.0014.
49. D. Dubois, N. Merbahi, O. Eichwald, M. Yousfi, and M. Benhenni, (2007) Electrical analysis of positive corona discharge in air and N₂, O₂, and CO₂ mixtures, *Journal of Applied Physics* 101, 053304
50. Chase S. Murray (2020) Evolution of Electron Properties After Nanosecond Repetitively Pulsed Discharges in Air Measured by Thomson Scattering, M.S, Thesis, Wright State University

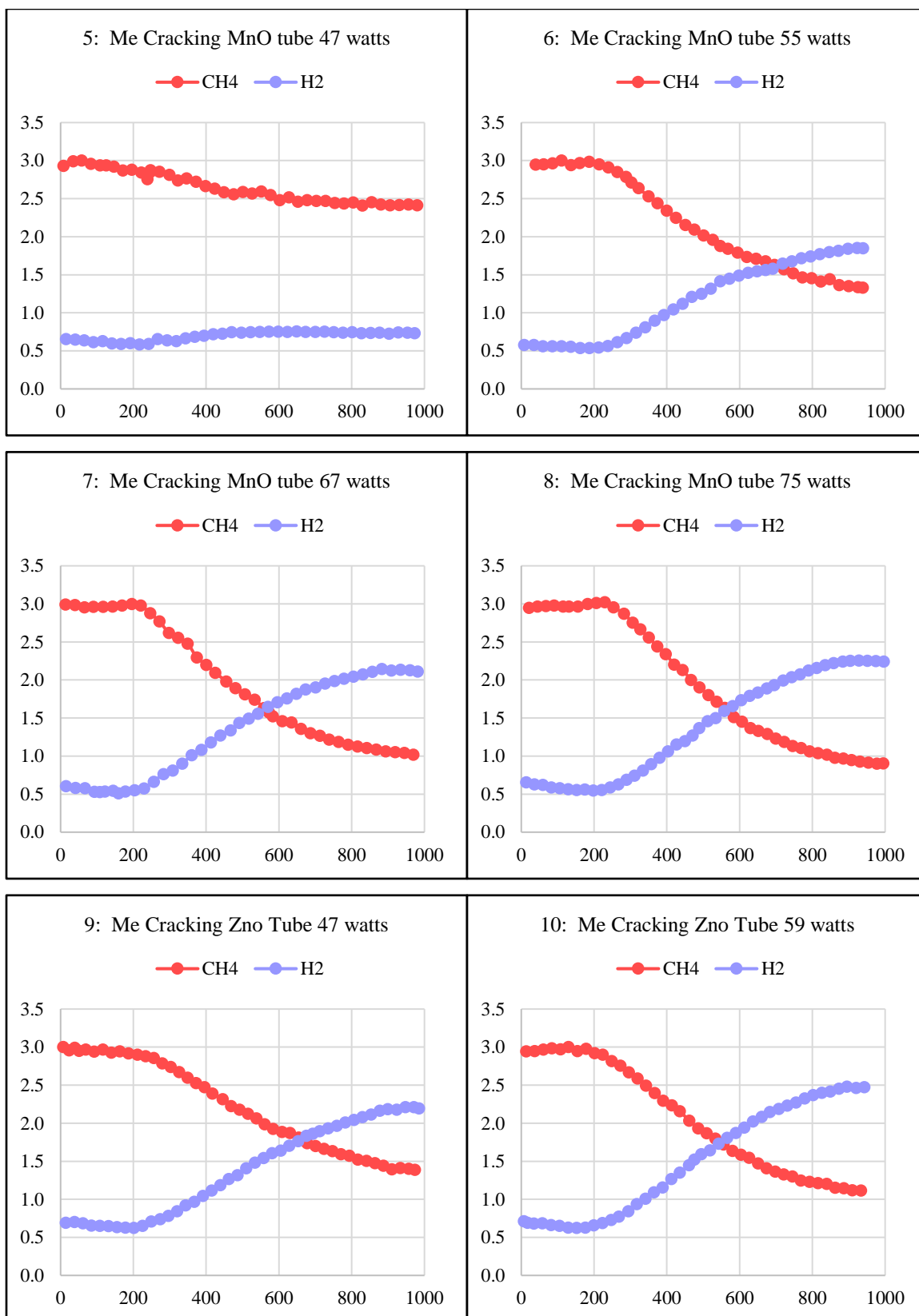
A Emission Spectra Reference Charts

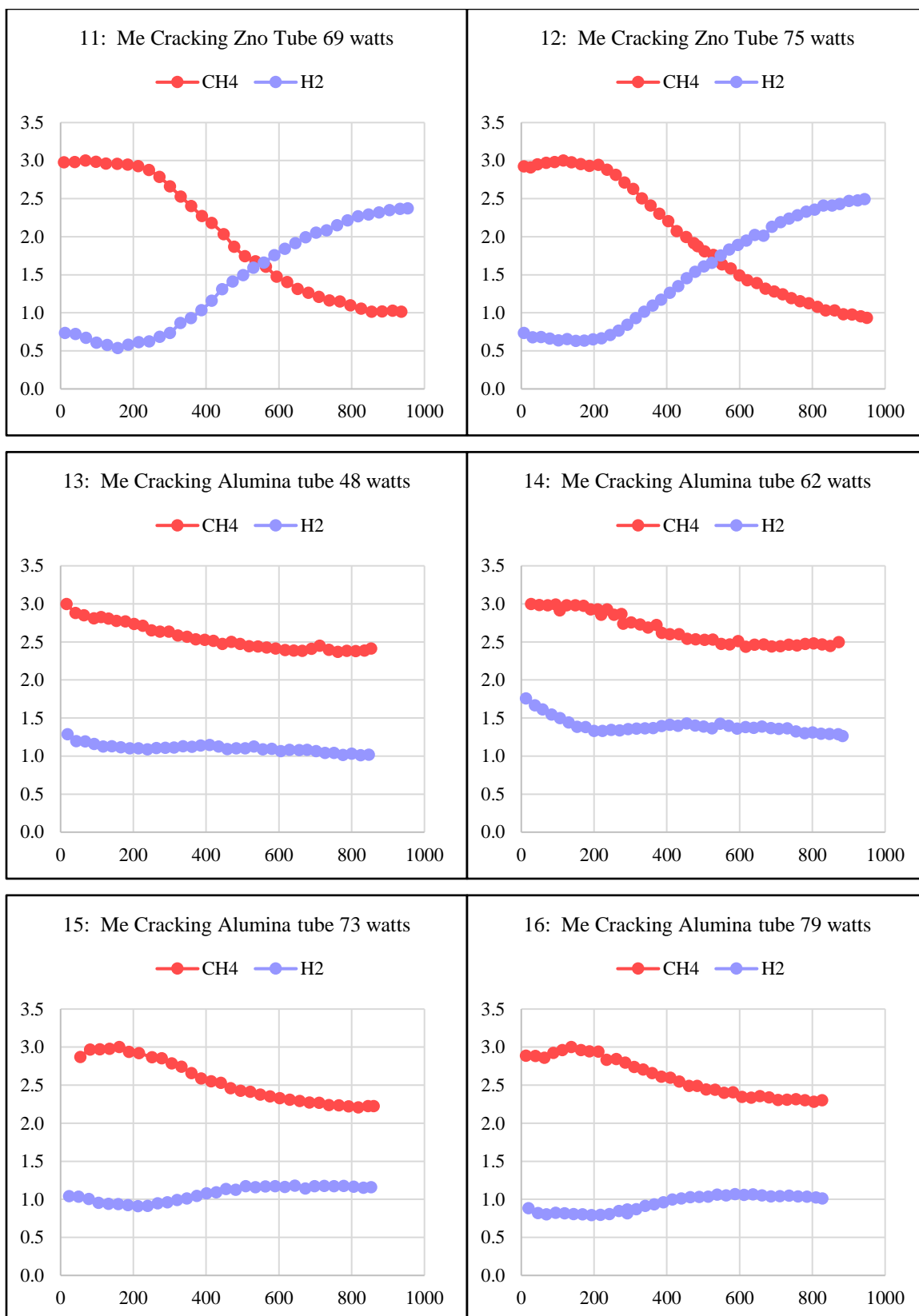


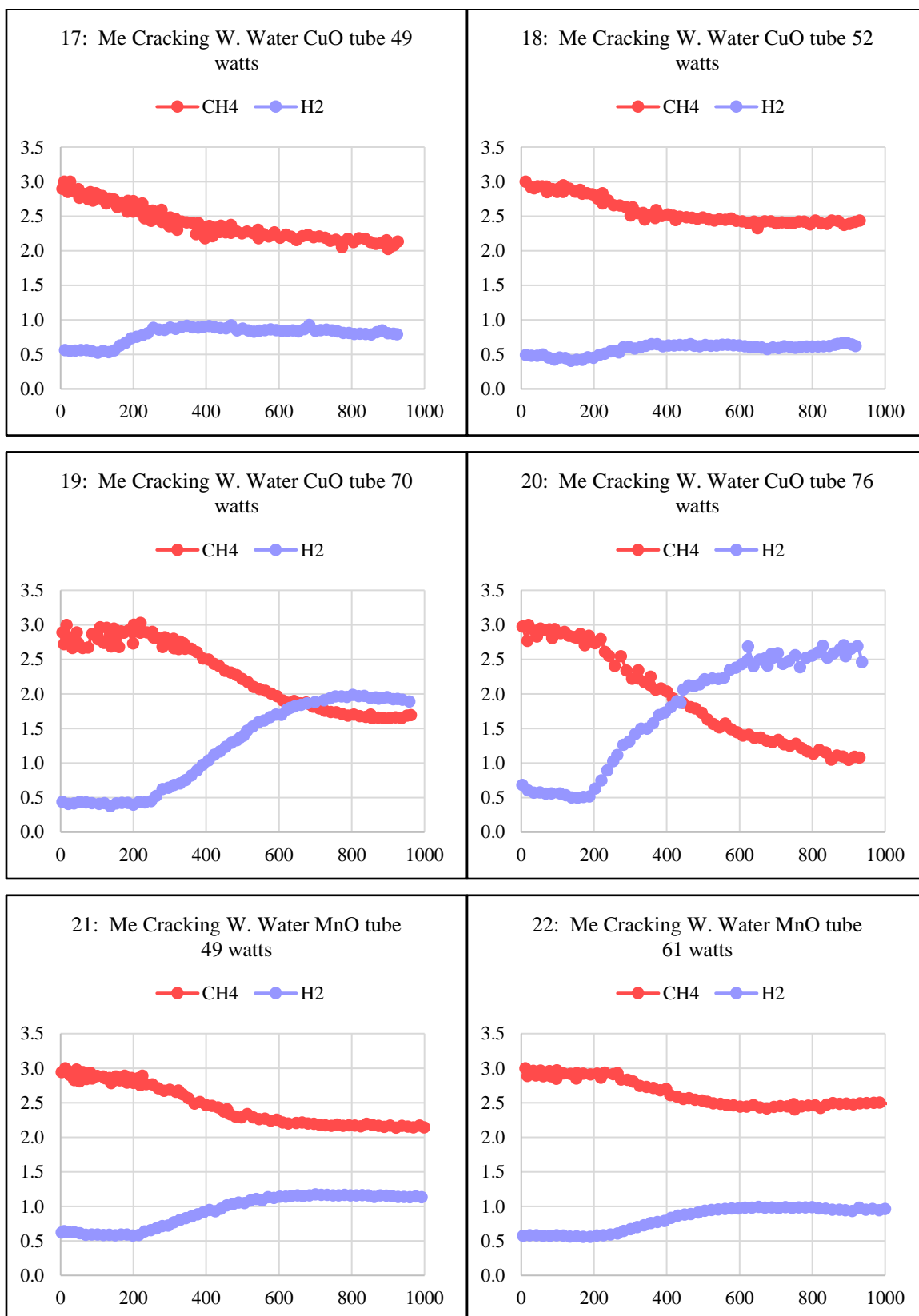
<https://www.semanticscholar.org/paper/One%E2%80%90Step-Reforming-of-CO2-and-CH4-into-High%E2%80%90Value-Wang->

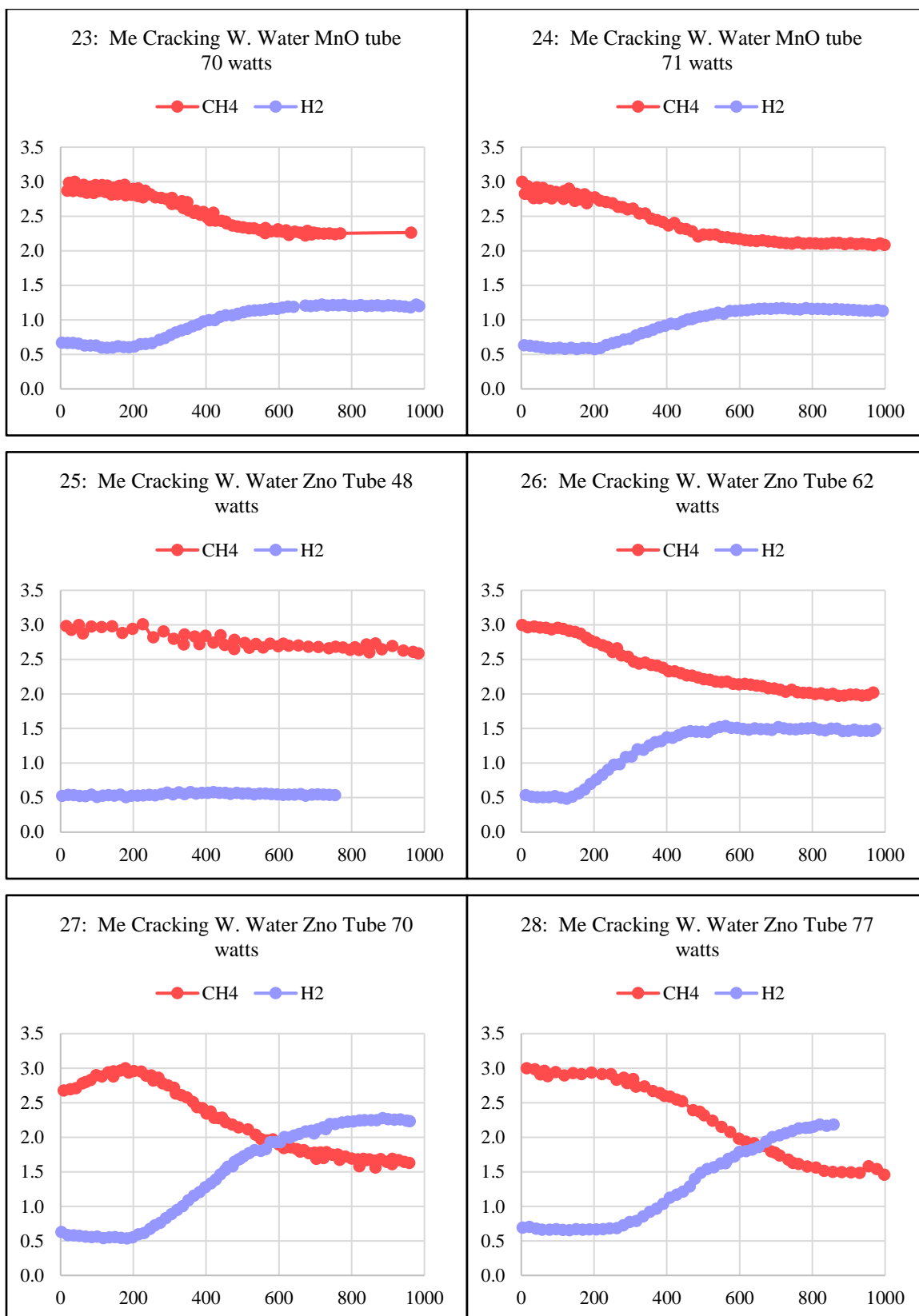
B Experimental Data

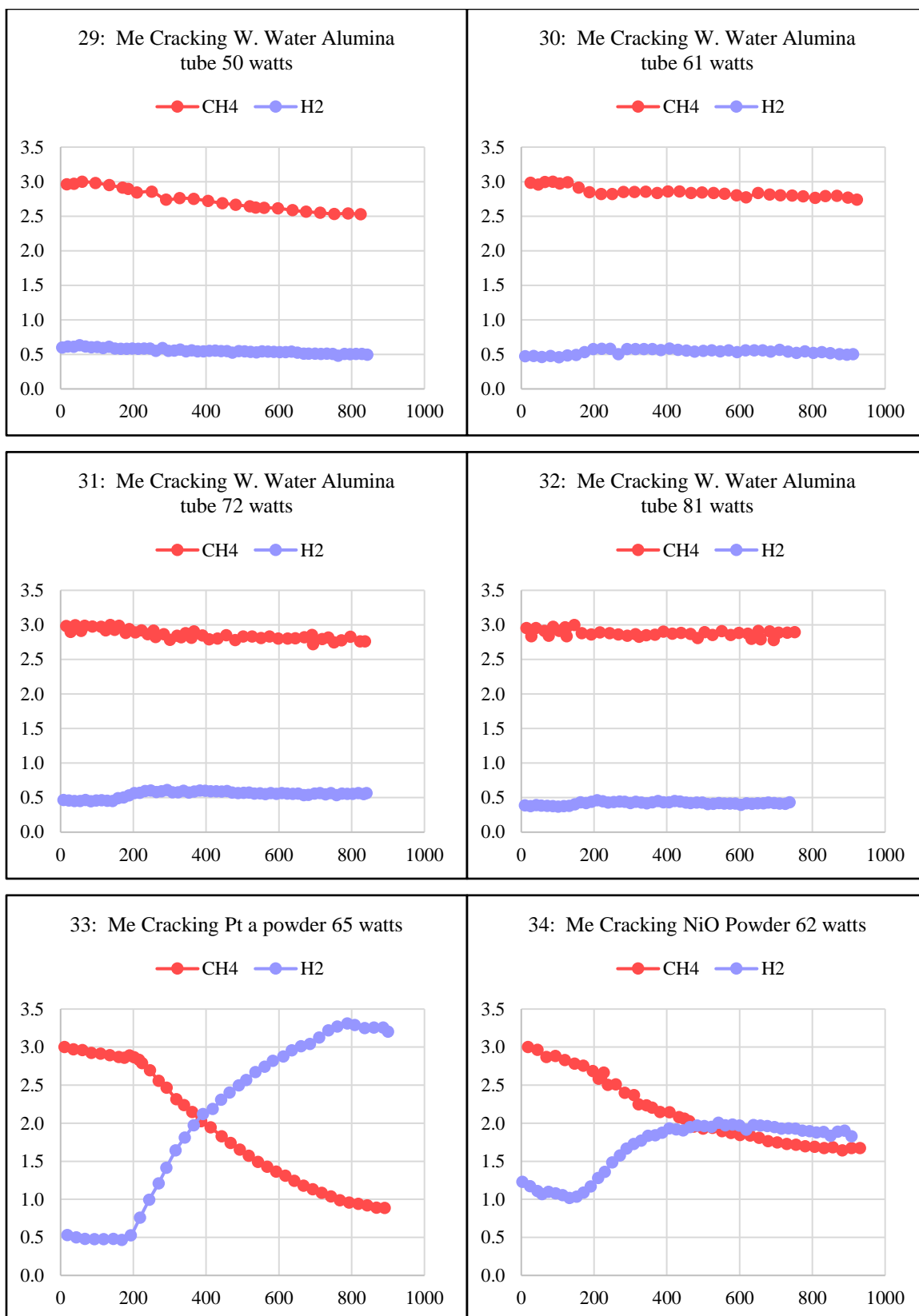


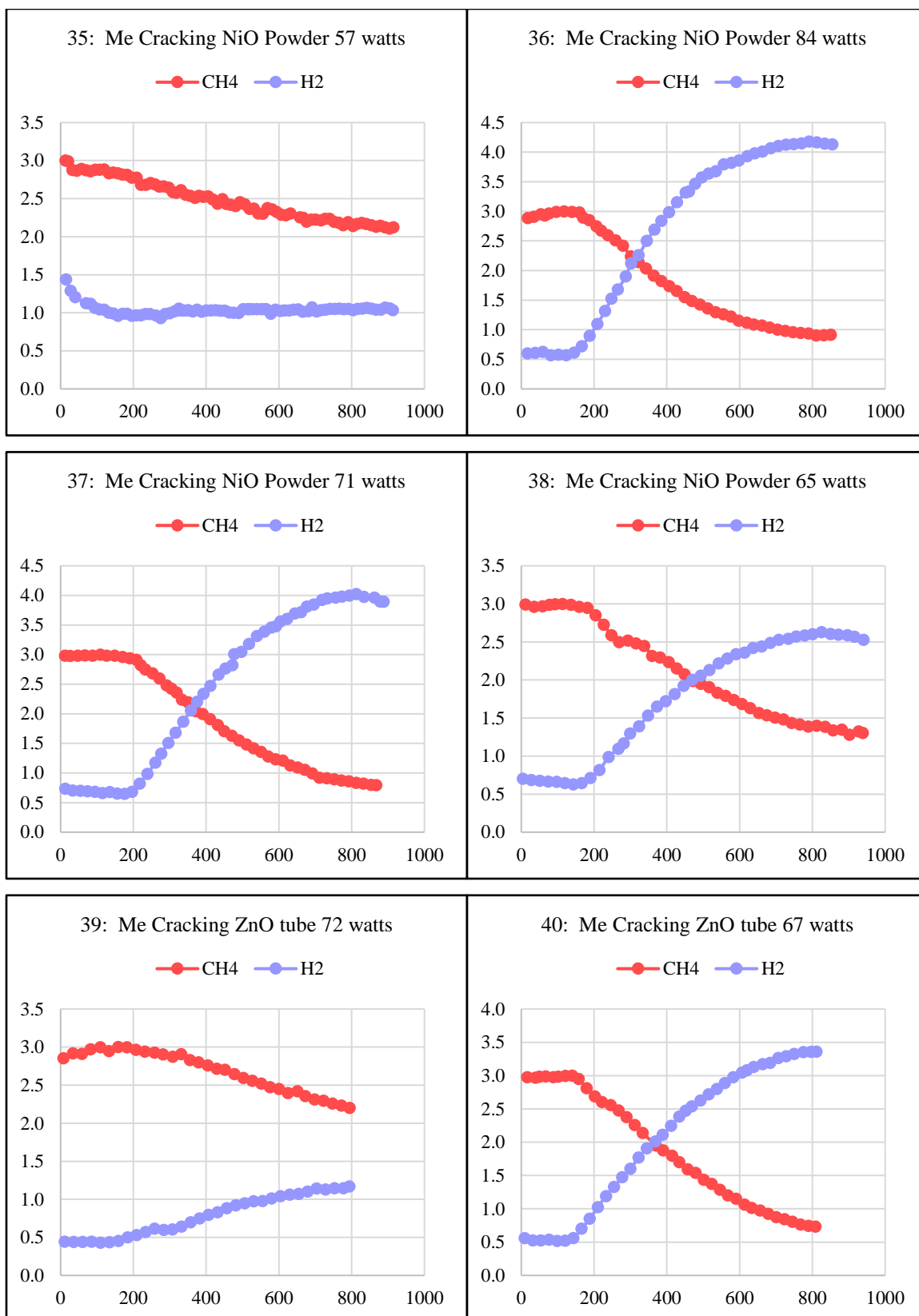


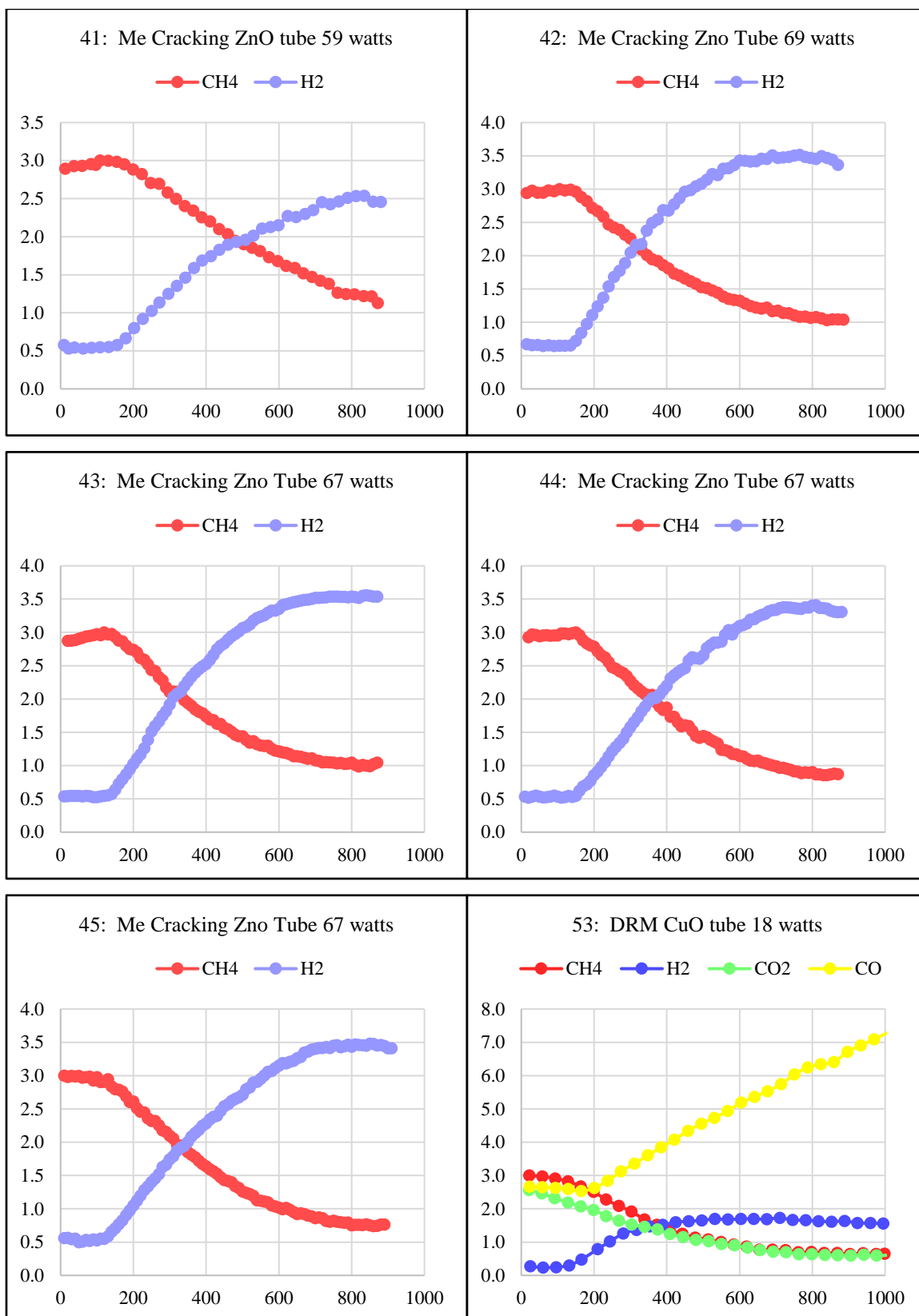


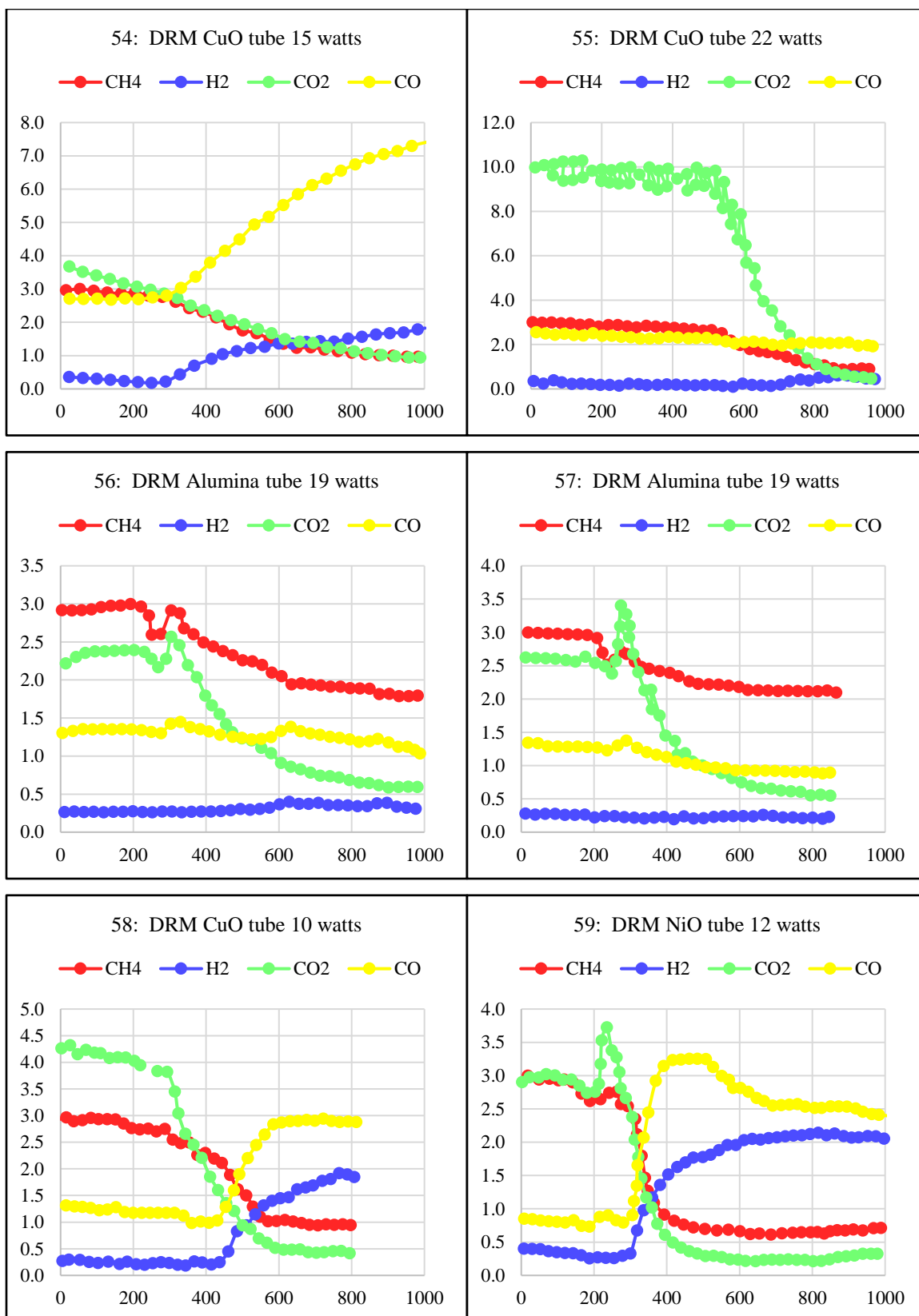


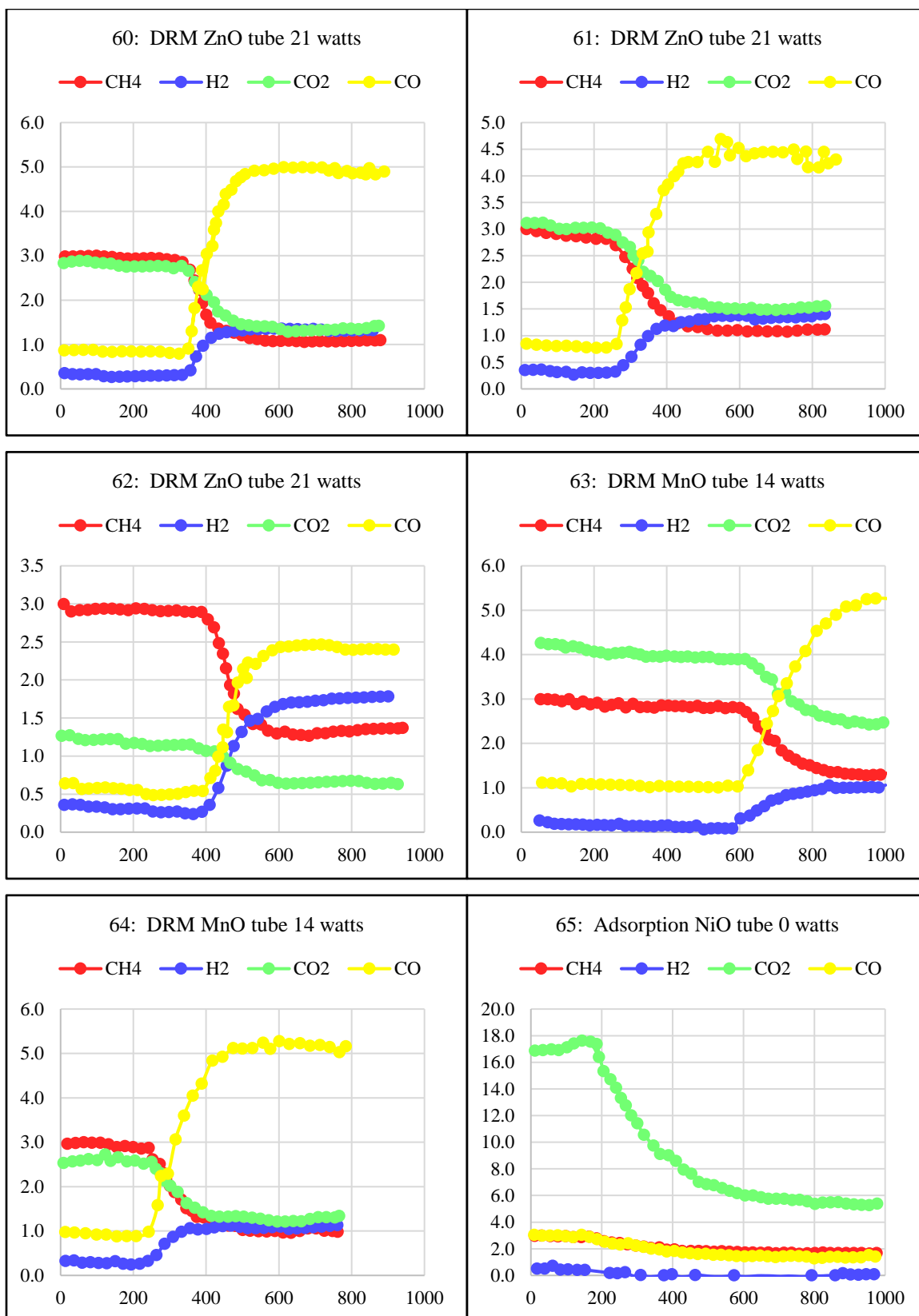


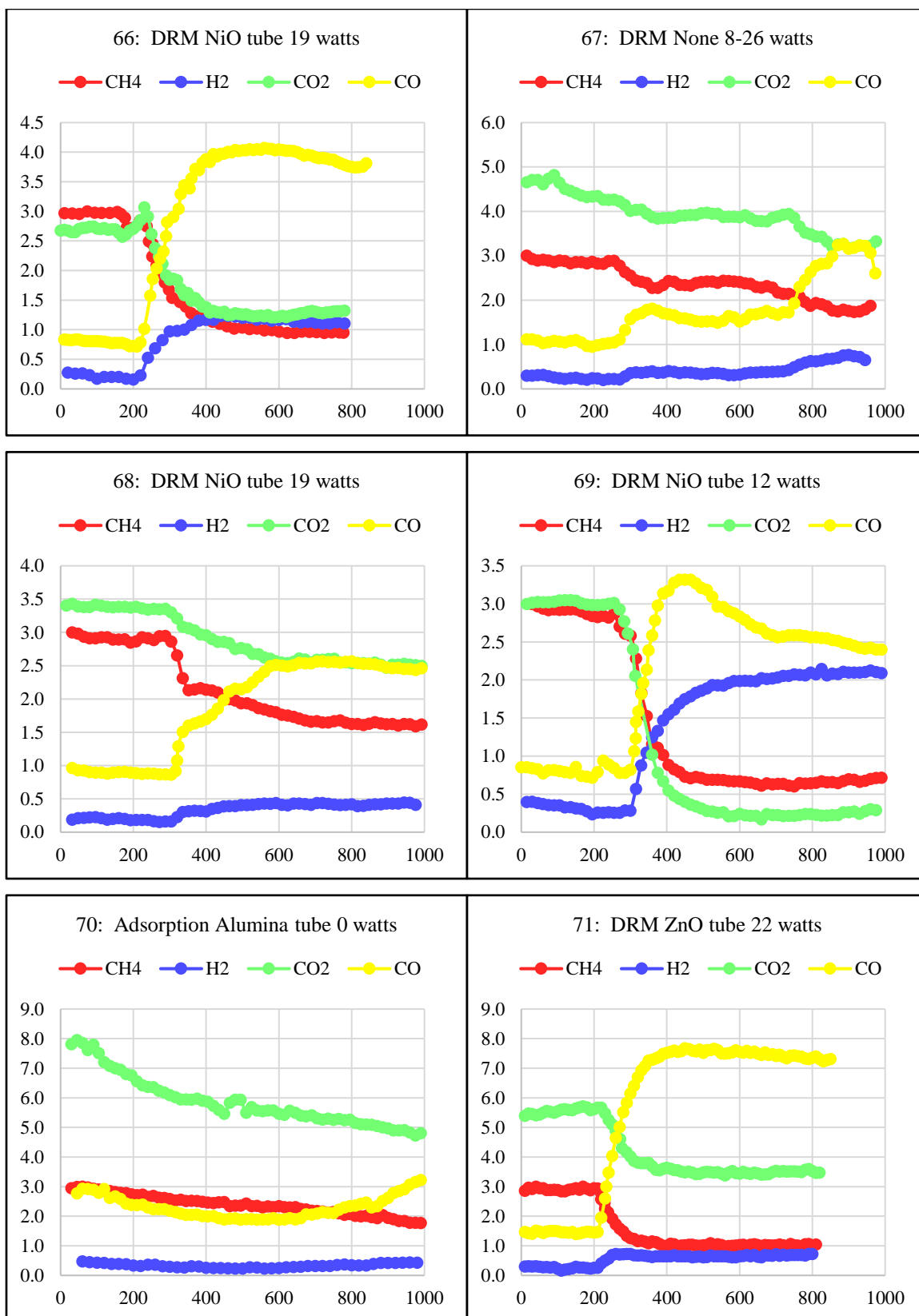


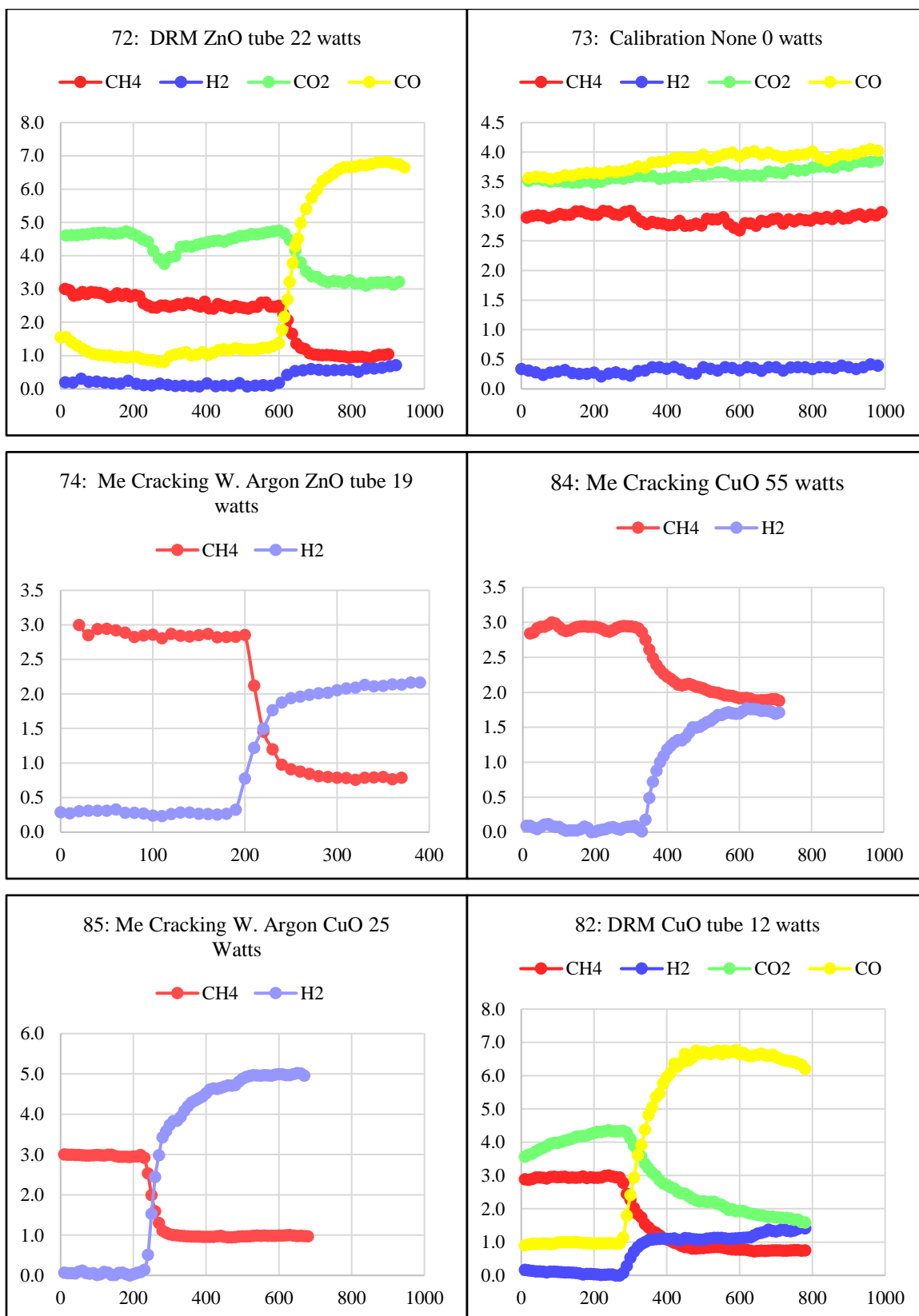


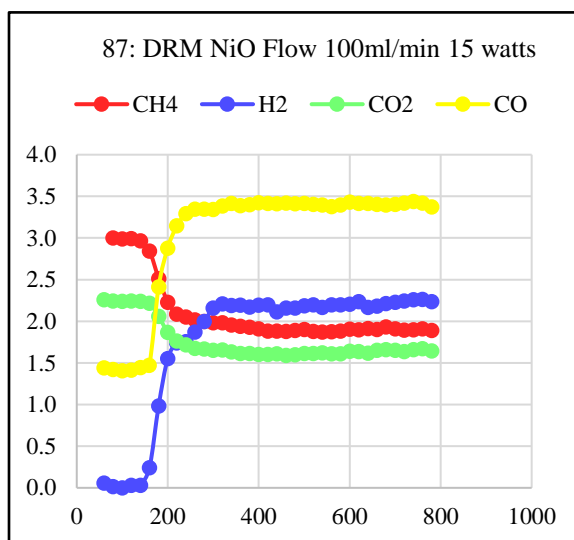
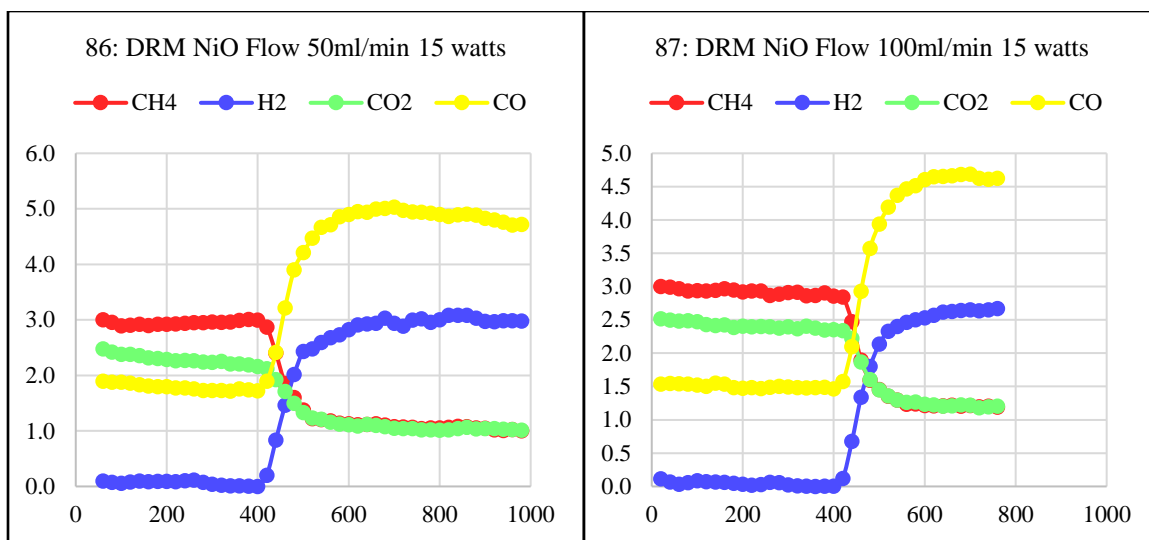








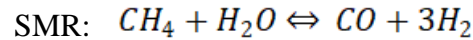
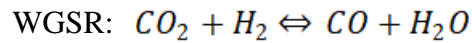
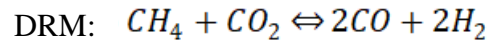




C Extend of Reaction through Gibb's Free Energy Minimalization

The non-thermal equilibrium nature of the non-thermal plasma DRM reaction can be confirmed by calculating the theoretical equilibrium extent of reactions and comparing to the observed values.

Assuming a 1 to 1 feed ratio of CH_4 to CO_2 and the following three equations:



The equilibrium composition was determined by Gibb's free energy minimalization via a Mathcad program. The extent of reaction was then determined from the equilibrium composition via an Excel program.

The equilibrium extent of reaction results are summarized in the following table:

Reaction	ΔG_{min} prediction at 25°C	Observed at 25°C for ZnO/CuO plasma DRM	ΔG_{min} prediction at 725°C
DRM	$2.19 \cdot 10^{-5}$	0.513	0.492
WGSR	$2.53 \cdot 10^{-5}$	0.121	0.186
SRM	0	0.102	$1.49 \cdot 10^{-4}$

This shows that the extent of reaction achieved in the plasma reactor at room temperature is far greater than would be predicted by traditional thermodynamics. The plasma reactor results are comparable to the predicted values at 725°C.